Geochemistry Geophysics Geosystems G3
AN ELECTRONIC JOURNAL OF THE EARTH SCIENCES
Published by AGU and the Geochemical Society

Article
Volume 5, Number 4
17 April 2004
Q04006, doi:10.1029/2003GC000618
ISSN: 1525-2027

Characteristics of deep (≥13 km) Hawaiian earthquakes and Hawaiian earthquakes west of 155.55°W

Cecily J. Wolfe
Hawaii Institute of Geophysics and Planetology, University of Hawaii at Manoa, Honolulu, Hawaii 96822, USA (cecily@soest.hawaii.edu)

Paul G. Okubo
Hawaiian Volcano Observatory, US Geological Survey, Hawaii National Park, Hawaii 96718, USA

Göran Ekström and Meredith Nettles
Department of Earth and Planetary Sciences, Harvard University, Cambridge, Massachusetts 02138, USA

Peter M. Shearer
Institute of Geophysics and Planetary Physics, Scripps Institution of Oceanography, University of California at San Diego, La Jolla, California 92093, USA

[1] High precision relocation of earthquakes recorded by the Hawaiian Volcano Observatory (HVO) seismic network provides new information on the characteristics of seismic faulting at this oceanic hot spot. Using waveform cross correlation, we have measured correlation coefficients and travel time differences for a set of 14,605 deep (≥13 km) earthquakes recorded from 1988 to 1998. We find that about half of the analyzed earthquakes are in similar event clusters that delineate fault zones in the lower crust and upper mantle. We suggest that much of this deep seismicity reflects rupture in the brittle lithosphere away from the magma pathways, although at Kilauea the stresses from magma movement may additionally help trigger mantle earthquakes on preexisting faults in regions with high differential ambient stresses. Focal mechanisms of similar event clusters throughout Hawaii display characteristic patterns and appear consistent with the hypothesis that deep earthquakes on preexisting faults reflect the stresses due to volcano loading and flexure. We also present the results of applying cross correlation analyses and relocation to ~7000 earthquakes at all depths located west of 155.55°W and recorded from 1988 to 1998. The pattern of relocated earthquakes at the Kealakekua fault zone is consistent with the presence of a low-angle detachment on the west flank of Mauna Loa.

Components: 11,212 words, 20 figures, 2 tables.

Keywords: Earthquakes; Hawaii.

Index Terms: 7230 Seismology: Seismicity and seismotectonics; 7280 Seismology: Volcano seismology (8419); 8123 Tectonophysics: Dynamics, seismotectonics.

Received 13 August 2003; **Revised** 17 February 2004; **Accepted** 3 March 2004; **Published** 17 April 2004.

Wolfe, C. J., P. G. Okubo, G. Ekström, M. Nettles, and P. M. Shearer (2004), Characteristics of deep (≥13 km) Hawaiian earthquakes and Hawaiian earthquakes west of 155.55°W, *Geochem. Geophys. Geosyst.*, *5*, Q04006, doi:10.1029/2003GC000618.

1. Introduction

[2] Hawaiian earthquakes have been extensively studied using local seismicity data, teleseismic waveform modeling, and historical analyses [e.g., *Eaton and Murata*, 1960; *Butler*, 1982; *Aki and Koyanagi*, 1981; *Klein et al.*, 1987; *Ryan*, 1988; *Gillard et al.*, 1992; *Got et al.*, 1994; *Gillard et al.*, 1996; *Klein and Wright*, 2000; *Caplan-Auerbach and Duennebier*, 2001; *Got and Okubo*, 2003]. Earthquakes at Hawaii can be classified into several different types [*Klein et al.*, 1987]. There are shallow volcanic earthquakes under active calderas and rift zones associated with magma intrusions and eruptions [c.f., *Tilling and Dvorak*, 1993; *Rubin et al.*, 1998] and there are tectonic earthquakes, such as earthquakes on volcano flanks that release stresses imposed by volcano growth. Earthquake waveform characteristics also vary at Hawaii. High frequency earthquakes are associated with shear faulting, whereas tremor and long-period earthquakes, present both at crustal [e.g., *Goldstein and Chouet*, 1994] and mantle depths [*Aki and Koyanagi*, 1981], likely reflect the resonance of fluid-filled conduits [e.g., *Chouet*, 1996].

[3] Hawaiian earthquakes are ultimately linked to the stresses produced by the growing volcanoes, and must be viewed within the framework of volcanism in Hawaii. The island of Hawaii contains five major volcanoes: Kilauea, Mauna Loa, Mauna Kea, Hualalai, and Kohala [*Peterson and Moore*, 1987]. During the period of modern seismic monitoring (~1959-present), Kilauea has been the most active volcano, since 1983 erupting in the voluminous Pu'u 'O'o-Kupaianaha eruption. From 1832 to 1950 Mauna Loa erupted 35 times, or once every 3.4 years on average, but since 1950 it has only erupted twice, in 1975 and 1984. Hualalai is considered a dormant volcano, having last erupted ~200 years ago. Mauna Kea has been inactive for several thousands of years and Kohala has been inactive for more than sixty thousand years. To the southeast of Hawaii, Loihi seamount offshore is an active volcano that erupted in 1996 [*Garcia et al.*, 1998]. To the northwest of Hawaii, Haleakala on east Maui, is a dormant volcano, having last erupted ~200 years ago [c.f., *Bergmanis et al.*, 2000].

[4] Despite the low levels of volcanism outside of Kilauea and Mauna Loa, earthquakes occur throughout the island of Hawaii and its environs [*Klein et al.*, 1987], forming a complex pattern that could reflect a variety of causes, including magma movement, zones of structural weakness, stresses due to volcano loading and lithospheric flexure, and thermal cooling stresses. In this paper, we apply high precision earthquake relocation methods [c.f., *Got et al.*, 1994; *Gillard et al.*, 1996; *Shearer*, 1997; *Waldhauser and Ellsworth*, 2000; *Wolfe*, 2002] to obtain a more accurate picture of the characteristics of deep Hawaiian earthquakes ($\geq$13 km) as well as Hawaiian earthquakes west of 155.55°W. This study expands on the work of *Wolfe et al.* [2003], providing a more detailed description of the methods, data, and results as well as adding new analyses. While the study of *Wolfe et al.* [2003] focused on the characteristics of a mantle fault zone at 30-km depth beneath Kilauea, here we give a more detailed description of the analyses, report on the characteristics of deep earthquakes throughout Hawaii, and add a study of earthquakes at all depths west of 155.55°W (shallow events east of 155.55°W are too numerous to include in this study). We explore the patterns of deep earthquakes focusing on distinguishing magmatic versus tectonic events to understand how the growing volcanoes affect the lower crust and upper mantle. We present an analysis of earthquakes west of 155.55°W in order to determine whether the detachment fault model for crustal faulting on the south flank of Hawaii [c.f., *Swanson et al.*, 1976; *Denlinger and Okubo*, 1995; *Owen et al.*, 1995; *Delaney et al.*, 1990] also applies at the west flank of Mauna Loa, as has been previously suggested from analysis of the mechanism of the 1951 magnitude 6.9 Kona earthquake [*Beiser et al.*, 1994] and local fault plane solutions [*Gillard et al.*, 1992]. In addition, we present refined depth estimates for 13 moderate and large earthquakes, based on very-broad-band modeling of teleseismic waveforms [*Ekström*, 1989], and determine eight

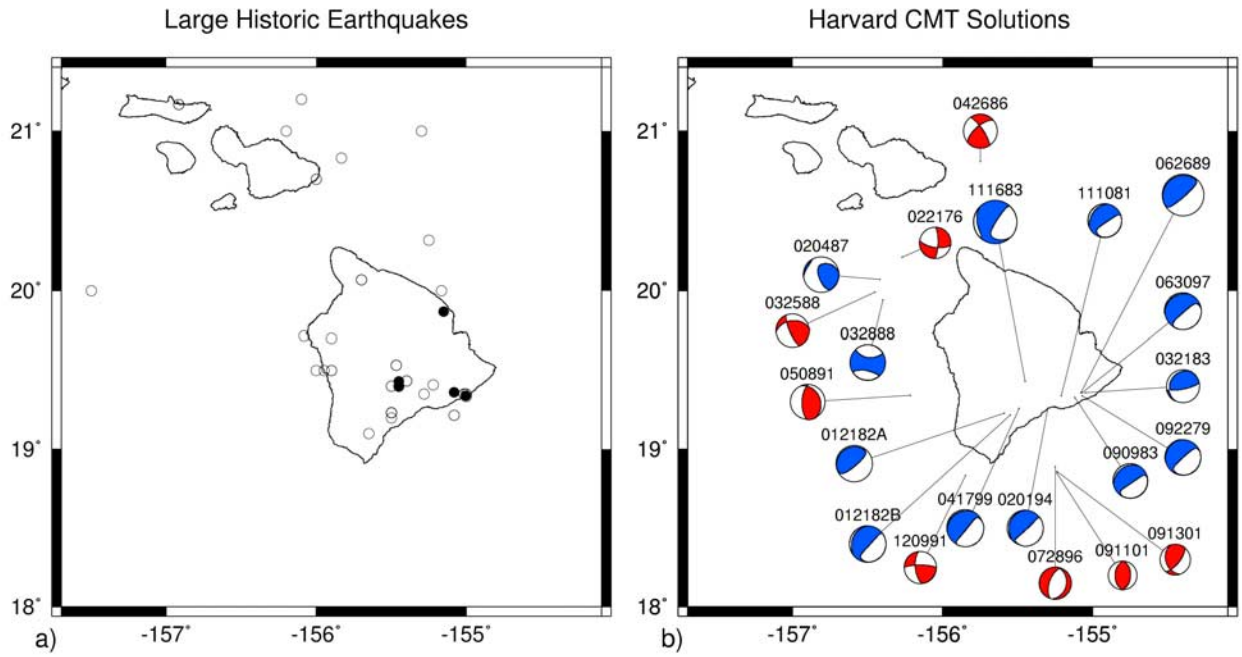

Figure 1. (a) Locations of large (magnitude $\geq$6.0) earthquakes since 1823: data from 1960–1997 are taken from the HVO earthquake catalog (solid circles), and data from 1823–1959 are taken from the historic catalog of *Klein and Wright* [2000] (open circles), which incorporates results from the earlier work of *Wyss and Koyanagi* [1992a]. We do not plot 12 earthquakes from *Klein and Wright* [2000] whose locations are poorly known: seven of these events are assigned in the catalog to south Hawaii, three of these events are assigned to west Hawaii, and one of these events is assigned to north Hawaii. Island coastlines are plotted as black lines. (b) Mechanisms of earthquakes in the Harvard Centroid Moment Tensor Catalog (blue) and mechanisms of M_w = 4.4–5.4 earthquakes determined in this study by modified CMT analysis (red), equal area lower-hemisphere projection. The caption above each earthquake displays the month, day, and year of the event. Further information on the determination of the new CMT solutions is given in the appendix.

new centroid moment tensor solutions for smaller events.

2. Background

[5] From the locations of major large (magnitude $\geq$ 6.0) earthquakes since 1823 (Figure 1a) [*Klein and Wright*, 2000], it is apparent that large earthquakes occur throughout the island of Hawaii, as well as in the regions around Maui and Molokai, although historic locations can be poor. Note that two historical earthquakes located in the Maui vicinity would be hazardous for Honolulu if they occurred today [*Klein et al.*, 2001]: the magnitude 6.8 1871 "Lanai" earthquake and the 1938 magnitude 6.8 offshore Maui earthquake. Large earthquakes are not confined to crustal faults and can be found in the underlying mantle. The 1973 magnitude 6.2 Honomu earthquake, which occurred at ~40–50 km depth beneath the northeast coast of Hawaii, in the Mauna Kea region, had an oblique strike-slip faulting mechanism [*Unger and Ward*, 1979; *Butler*, 1982; *Chen et al.*, 1990] and caused $4 million in damage around Hilo.

[6] Figure 1b shows the locations and focal mechanisms of Hawaiian earthquakes since 1976 in the Harvard Centroid Moment Tensor (CMT) catalogue as well as eight mechanisms obtained in this study from waveform modeling of smaller, M_w 4.4–5.4 earthquakes (see the appendix). Table 1 shows the depths of many of these earthquakes. Earthquakes with low-angle thrust faulting mechanisms and shallow hypocenters (mostly 7–10 km depth) occur on the southeast slopes of both Kilauea and Mauna Loa, and a similar type of mechanism has been obtained for the 1975 Kalapana earthquake [*Nettles and Ekström*, 2004]. These earthquakes likely reflect movement on a

Table 1. Centroid Depths of Recent Large Earthquakes[a]

Date	Depth, km
09/22/1979	8.1
11/10/1981	7.3
01/21/1982A	9.4
01/21/1982B	8.2
09/09/1983	8.2
11/16/1983	8.6
02/04/1987	9.5
03/28/1988	9.6
06/26/1989	13.1
05/08/1991	27.6
02/01/1994	30.8
06/30/1997	8.9
04/17/1999	8.3

[a] See Figure 1b. From the method of *Ekström* [1989].

low-angle decollement at the interface between the volcano and the preexisting oceanic crust [*Swanson et al.*, 1976; *Denlinger and Okubo*, 1995; *Owen et al.*, 1995; *Delaney et al.*, 1990].

[7] However, one low-angle faulting m_b 5.3 earthquake at Kilauea, on February 2, 1994, occurred in the mantle at about 30 kilometers depth rather than within the crust. Figure 2 shows the pattern of local magnitude $m_L \geq 3$ earthquakes in the depth interval 20–40 km from the available HVO catalog of larger ($\sim m_L \geq 1.5$) earthquakes from October 1959 through 2000. Since HVO obtains two estimates of local magnitudes, one using seismic coda and the other using seismic amplitudes, we take as m_L either the preferred HVO magnitude, if listed, or the larger of the coda and the amplitude magnitudes (only amplitude magnitudes were calculated by HVO prior to 1974). As observed by *Wolfe et al.* [2003], there is a highly active deep seismic zone associated with Kilauea volcano (Figures 2 and 3). Of the 1011 $m_L \geq 3$ Hawaiian earthquakes in this depth and time interval, 42% occur in the Kilauea region (shown in Figure 3b), making it by far the most seismically active region at depths of 20–40 km. The large numbers of $m_L \geq 3$ earthquakes suggest a zone of deep faulting at Kilauea.

[8] Plots of the cumulative number of events versus time for depths of 20–40 km beneath Kilauea (Figure 4) reveal that this area generally experiences a steady rate of earthquakes rather than swarm behavior, although the aftershocks of the 1994 earthquake generated a small rate increase for a short period in 1994. These characteristics are typical of tectonic earthquakes. While the time interval and spatial region we examined did not display swarms, occasional earthquake swarms at depths of 45–65 km were observed from the early 1950s until late in 1960 [*Eaton and Murata*, 1960; *Eaton et al.*, 1987], so the characteristics of deep seismicity beneath Kilauea may change with time. The rate of earthquakes and the magnitude characteristics of earthquakes substantially changed in 1975, after the magnitude 7.5 Kalapana earthquake, which occurred at 9 km depth along the south flank at Kilauea. Although there may be issues in terms of the completeness of this catalog, as illustrated by a comparison between Figures 4a and 4c, this change could reflect the influence of a change in stress on the earthquake rates [*Dieterich et al.*, 2000] of the deep fault system. Deep earthquakes are not confined to the Kilauea region but occur throughout much of Hawaii (Figure 2).

3. Relocation of Deep Earthquakes

[9] The accuracy of routinely determined hypocenters is limited by factors including the network geometry, the available arrival time picks, picking errors, and the presence of three-dimensional

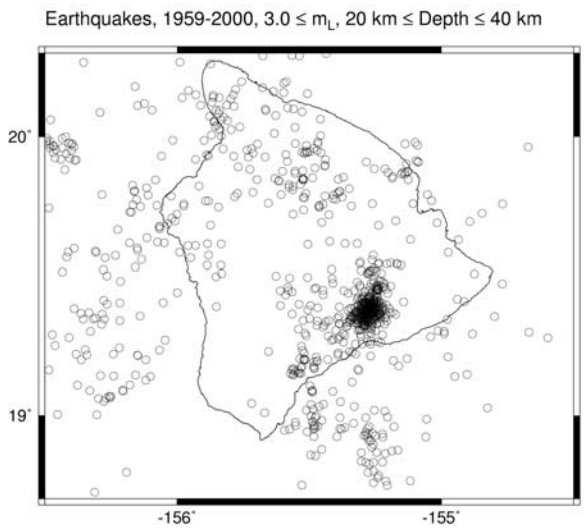

Figure 2. Plot of $m_L \geq 3$ earthquakes in the depth interval 20–40 km from the available HVO catalog of larger ($\sim m_L \geq 1.5$) earthquakes from October 1959 through 2000.

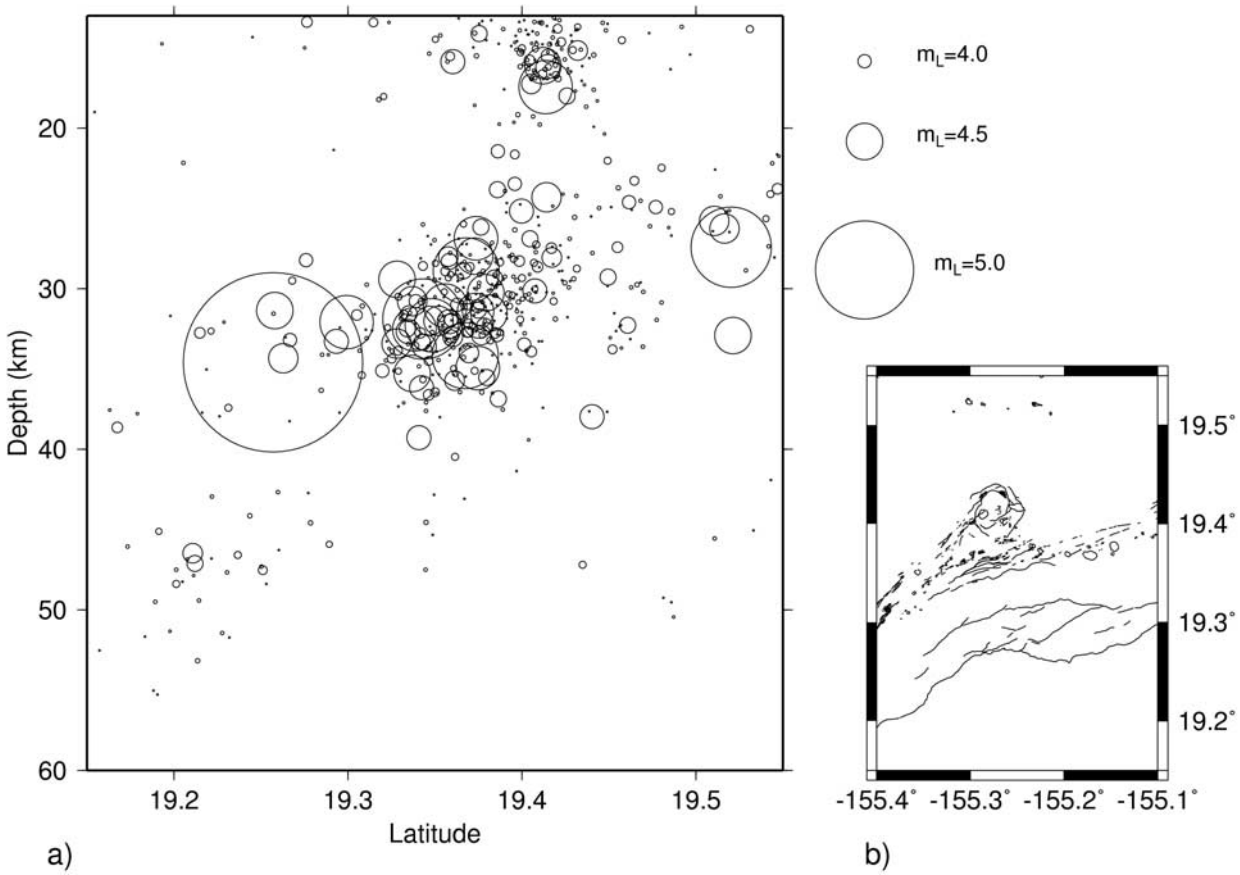

Figure 3. (a) Plot of $m_L \geq 3$ earthquakes in the region of Kilauea shown in Figure 3b. (b) Region of Kilauea with geologic features shown as lines.

velocity heterogeneity. Thus relocations of earthquakes using relative location methods, which reduce the effects of velocity heterogeneity, combined with precise cross correlation measurements have produced more accurate locations [*Got*, 1994; *Gillard et al.*, 1996; *Shearer*, 1997; *Rubin et al.*, 1998, 1999; *Waldhauser and Ellsworth*, 2000] and delineated fault structures. In this section, we discuss how we have applied high precision relocation methods to data from Hawaii.

[10] If two earthquakes are closely spaced compared to the scale of three-dimensional velocity heterogeneity, then the path anomalies from heterogeneity are similar. There are two types of methods developed to improve the relative locations in this situation: one approach is to estimate and remove station corrections from source regions when relocating earthquakes [e.g., *Shearer*, 1997; *Richards-Dinger and Shearer*, 2000] and the other approach is to relocate earthquakes using travel time differences [e.g., *Jordan and Sverdrup*, 1981; *Got et al.*, 1994; *Shearer*, 1998; *Waldhauser and Ellsworth*, 2000; *Wolfe*, 2002]. The data used in these methods can be either hand picked travel times or, in the case of differencing methods, cross-correlation travel time differences.

3.1. Relocation Using Travel Time Data

[11] We initially relocated deep earthquakes at Kilauea using an available catalog of HVO hand-picked arrival time and first motion polarity data for earthquakes $\sim m_L > 1.5$ from 1974–2000. Throughout this study, stations are distinguished according to the three letter station name, although there are cases where several different stations, with different station names, have occupied the same site. We used the double difference method of *Waldhauser and Ellsworth* [2000] as well as the

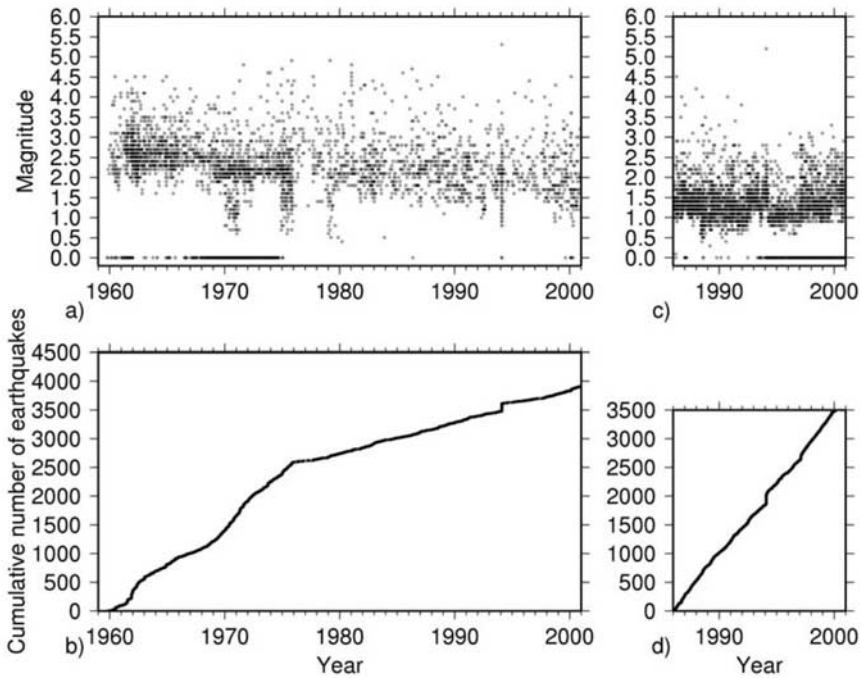

Figure 4. (a) The magnitudes of earthquakes versus time in the Kilauea region (Figure 3b) at depths of 20–40 km from 1959–2000. Data are from the HVO catalog of $\sim m_L > 1.5$ earthquakes. (b) Cumulative number of earthquakes versus time for the data in Figure 4a. (c) The magnitudes of earthquakes versus time in the Kilauea region at depths of 20–40 km from 1986–2000. Data are from the internal HVO catalog, which contains the HVO initial estimate of location and magnitude for all located earthquakes, with no magnitude cutoff. (d) Cumulative number of earthquakes versus time for the data in Figure 4c.

source specific station term method of *Richards-Dinger and Shearer* [2000], although the results from both methods are qualitatively similar. An example set of relocated earthquakes is shown in Figure 5. The set of earthquakes near 30 km depth collapses after relocation to a feature more localized in depth. Also, some clusters of earthquakes become more point-like features after relocation. These patterns are confirmed and mapped in greater detail when using high precision cross correlation travel time differences, as discussed in the following sections.

3.2. Relocation Using Cross Correlation Data

[12] When waveforms from earthquakes are highly similar, the errors in hand picking phase arrival times from earthquakes can be significantly reduced by using high-precision travel time differences from waveform cross correlation [*Poupinet et al.*, 1984]. Cross correlation measurements are particularly important for *S* waves, whose often emergent signals are difficult to accurately pick. In this section, we apply relocation methods using travel time differences from waveform cross correlation.

[13] We first consider waveforms from 1988–1998 in the full catalog of routinely located deep earthquakes recorded by the HVO seismic network, amounting to 14,604 events spread across and around Hawaii. On the basis of waveform characteristics, seismic events at Hawaii can be classified into three types: high frequency earthquakes that indicate shear faulting, and long-period (LP) earthquakes and tremor [*Aki and Koyanagi*, 1981; *Koyanagi et al.*, 1987; *Chouet*, 1996] that likely reflect resonance in fluid-filled conduits. The data set of deep earthquakes contains 2376 LP events, with 90% above 20-km depth, and 135 tremor events, with 90% below 30-km depth. Note that the subjective identification of LP events and tremor is made at HVO as part of their operations.

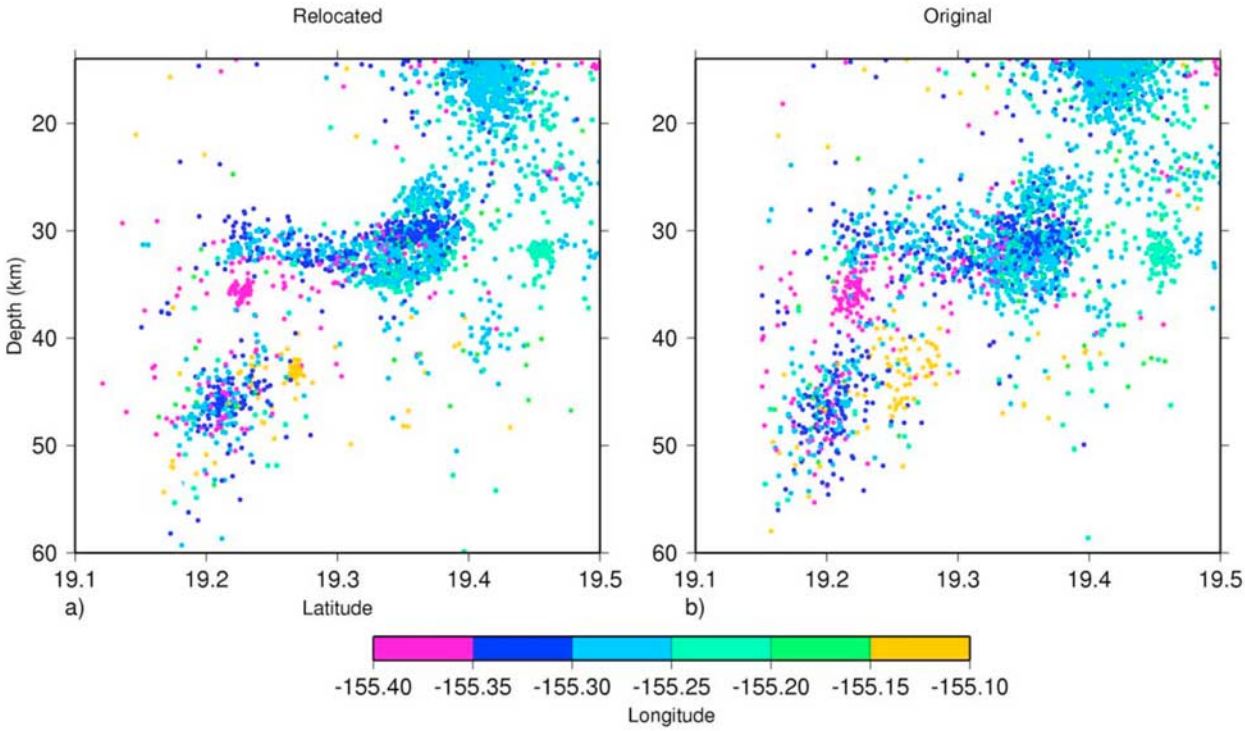

Figure 5. (a) Relocated earthquakes using travel time data and the method of *Waldhauser and Ellsworth* [2000] for the region in Figure 3b. Hypocenters are plotted in a vertical cross section of latitude versus depth, and circles are colored according to longitude. (b) Original catalog locations.

The catalog we used only includes located LP events and tremor and does not include events that could not be picked and located.

[14] Precise arrival time differences for earthquake pairs were first obtained using waveform cross correlation with parameters appropriate for high frequency earthquakes. For all possible earthquake pairs with catalog distances less than 10 km apart, waveforms on the vertical component were filtered to 2–15 Hz, sliced in 3 s (300 time sample) windows around the predicted *P* and *S* arrival times, and common phases on common stations were cross correlated to obtain arrival time differences. The analysis was restricted to the vertical components because only 14 of the 54 stations used were equipped with three components. Two events were considered similar if at least 10 waveform pairs equaled or exceeded a cross-correlation threshold of 0.6. We also required that the cross correlation function have negative values within 80 ms of the correlation peak and that the function not contain multiple oscillations above the threshold level. This restriction is designed to weed out false correlation peaks, such as from the alignment of data glitches or from the alignment of microseismic noise on seismograms with poor signal-to-noise ratio.

[15] The choice of cross-correlation threshold affects the number of relocated earthquakes. In order to investigate patterns in our data and the influence of the cross-correlation threshold, we first perform an L1 norm grid search relative relocation for all correlated earthquake pairs [*Shearer*, 1998]. That is, for every earthquake pair satisfying our similarity criteria, we can relocate that pair relative to the centroid of the starting locations using just the cross-correlation travel time differences for that pair. As explained by *Shearer* [1998], these results form a set of unreconciled estimates of the differential locations between the earthquake pairs analyzed. For example, if for N earthquakes, all possible N(N-1)/2 pair combinations yielded quality cross correlation data, the unreconciled relocations would produce N(N-1)/2 estimates of the differential locations between these pair combinations, many more than the needed N

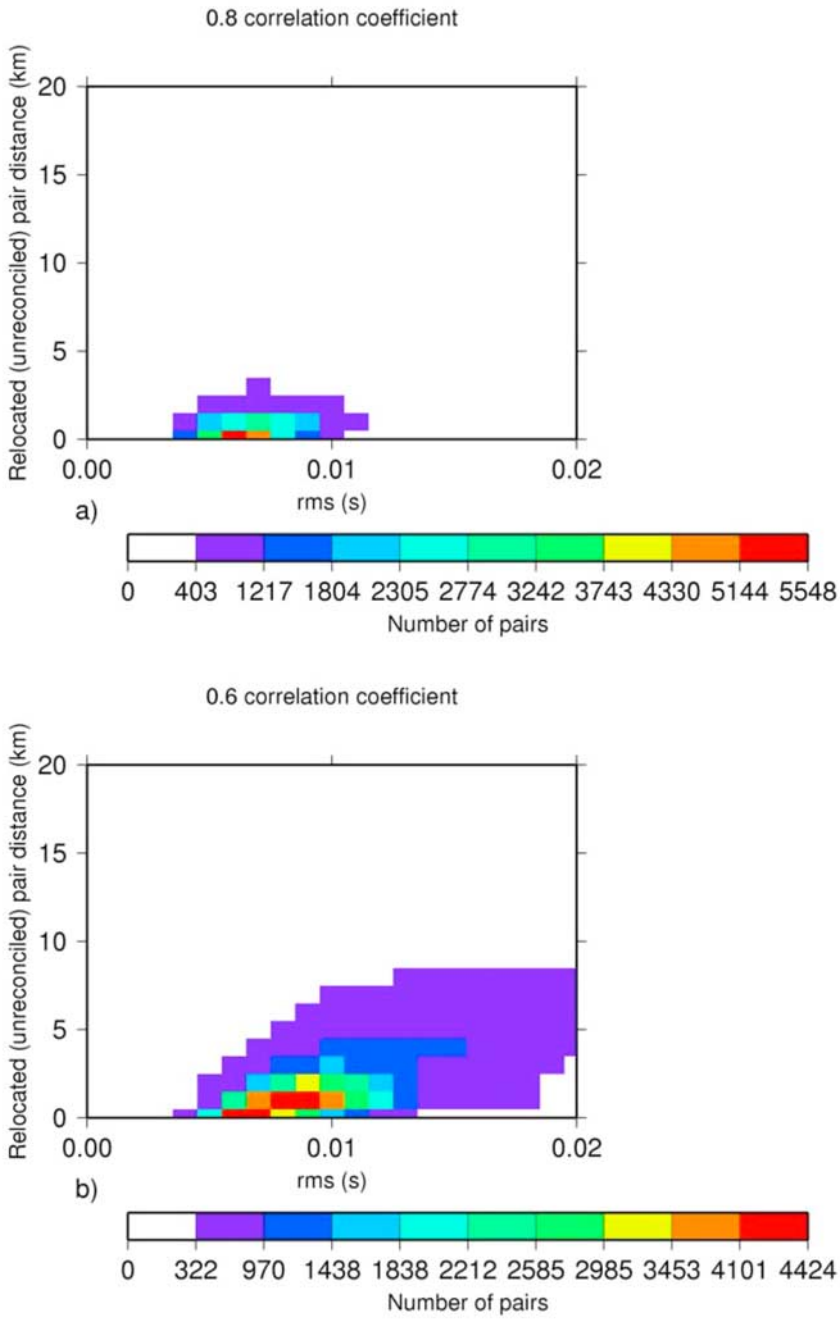

Figure 6. Plots of the L1 norm grid search relocation pair distance versus RMS error of the solution. Data are binned in centered intervals of 1 km in distance and 1 ms in time. (a) Cross correlation threshold of 0.8. (b) Cross correlation threshold of 0.6.

locations. Methods that directly invert the travel time differences for relocations [e.g., *Got et al.*, 1994; *Waldhauser and Ellsworth*, 2000] or that invert the unreconciled differential locations for a single best-fitting set of relative locations [*Shearer*, 1998] reconcile all of the redundancy in the differential travel times. The advantage of initially looking at the data characteristics using the L1 norm unreconciled relocations is that each pair of estimated differential locations is independent, and thus the presence of poorly constrained pairs has no effect on the relocations of other pairs. An L1

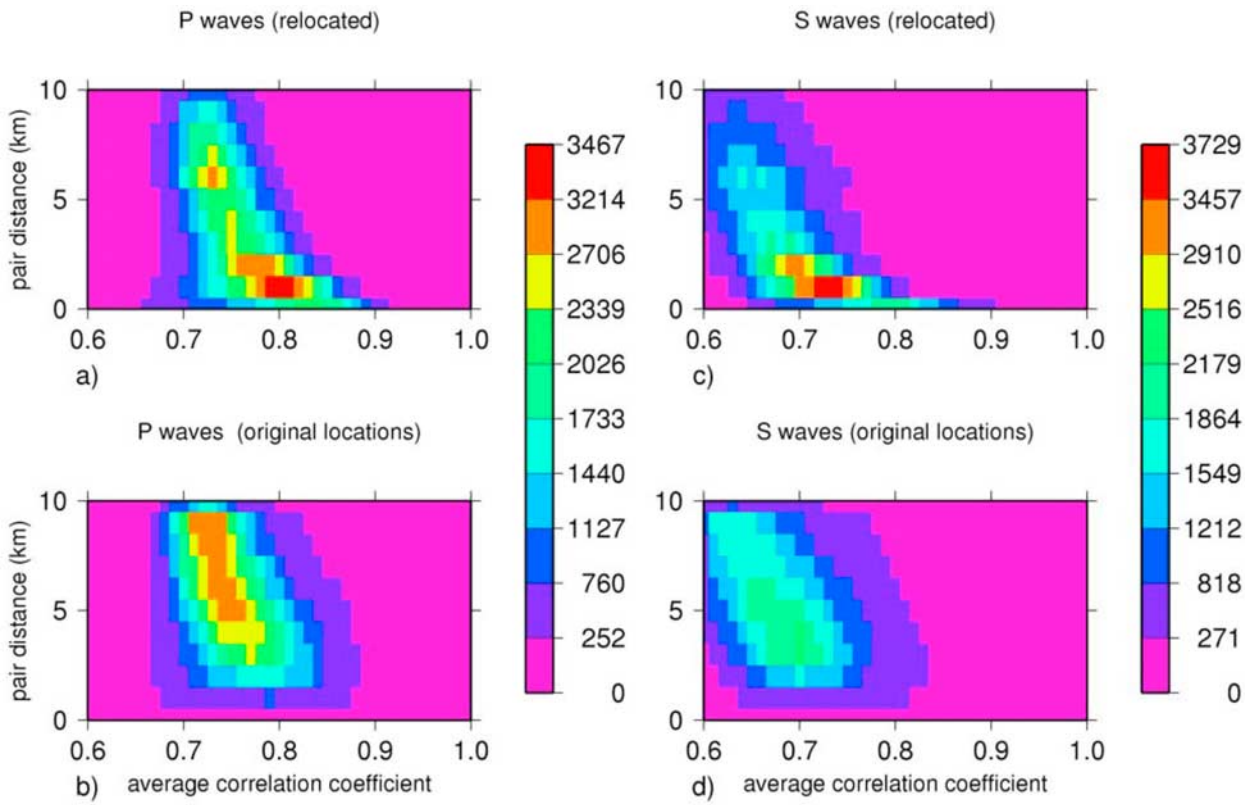

Figure 7. Plots of the pair distance versus the average cross correlation coefficient of the data. A cross correlation threshold of 0.6 is used. Distances are binned in centered intervals 1 km wide and cross correlation coefficients are binned in centered intervals 0.01 wide. (a) Results using *P* waves and unreconciled relocations. (b) Results using *P* waves and original catalog locations. (c) Results using *S* waves and unreconciled relocations. (d) Results using *S* waves and original catalog locations.

norm minimization method has the additional advantage that it is more robust with respect to data outliers than an L2 norm minimization.

[16] Figure 6 shows a plot of the L1 norm grid search unreconciled pair distance versus the root-mean square (rms) error for all pairs analyzed, both for a cross-correlation coefficient threshold of 0.8 (Figure 6a) and 0.6 (Figure 6b). When the cross-correlation coefficient threshold is set to 0.8, relocated earthquake pairs occur most frequently in bins of 0–0.5 km separation distance with RMS of 5–7 ms, although there is also a significant frequency of pairs in bins of 0.5–1.5 km with RMS 5–9 ms. When the cross-correlation coefficient threshold is lowered to 0.6, the number of relocated pairs at close distances (<2.5 km) is significantly increased, but we also obtain a large number of pairs at interevent distances of 2.5–9.5 km.

[17] Figure 7 displays plots of the pair distance versus average correlation coefficient (with 0.6 coefficient threshold) for both *P* and *S* waves as well as catalog and relocated pair distances. The original catalog locations yield very few pairs with interevent distances less then 1.5 km (Figures 7b and 7d), although the average cross-correlation coefficient does decrease with pair distance, as would be expected from the effects of scattering [*Menke*, 1999]. Figures 7a and 7c show the pattern of the average cross-correlation coefficient versus distance when the events are relocated, which in contrast shows a high frequency of events at close distances (<2.5 km). In this case, at close distances (<2.5 km), the average cross correlation coefficient decreases rapidly with distance, whereas at further distances (>2.5 km) it decreases more slowly. An analogous type of pattern has been observed for earthquakes at Parkfield [*Nadeau et al.*, 1995]. Our

analysis of original catalog pair distance versus the relocated distance demonstrates that beyond 6.5 km catalog pair distance, few pairs relocate at much shorter pair distances, which supports our choice of a 10 km catalog distance cutoff for the cross-correlation, since most correlated pairs are relatively mislocated by only a few kilometers.

[18] Because we are interested in relocating the maximum number of earthquakes possible, we analyze data with a cross correlation coefficient of 0.6. However, we found that relocations with the full data set were not successful in reducing the RMS error to the ~10 ms levels indicated in Figure 6b, nor were the patterns of relocated earthquakes qualitatively similar to the patterns found using data with a 0.8 correlation coefficient threshold. We believe problems occurred because earthquake pairs with large separation distance (>~2 km) were included. There are two reasons such data would impair the relocations. (1) Earthquake pairs at large distances are not true multiplets (events with very similar waveforms), thus the travel time difference will no longer depend only on the arrival time difference but can also be affected by the relative waveform shapes. This effect will reduce the accuracy of the travel time differences at larger distances. (2) At large distances, the assumption that the path anomalies for two earthquakes are similar will be less valid (see *Wolfe* [2002] for further discussion on the issue of how pair linkages operate). Both of these two effects likely contribute to the increase in RMS error with pair distance in Figure 6b.

[19] In order to reduce these effects, the relocations for a 0.6 cross correlation threshold used a filtered subset of event pairs, which only included a pair if its L1 norm, grid search, unreconciled relative locations from the cross-correlation data were less than 2 km apart. A second set of data was also examined where the cross-correlation threshold was raised to 0.8 with no removal of event pairs. The patterns of relocated deep earthquakes from both sets of data are similar, and do not affect our interpretations, although the data subset with a correlation threshold of 0.6 yields 30% more relocated earthquakes from lower signal-to-noise events. As discussed later, visualization of waveforms at individual stations using the predicted *P* wave arrival times can be used to confirm the accuracy of the relocations.

[20] Cross-correlation data were used to relocate deep earthquakes by both the method of *Waldhauser and Ellsworth* [2000] and that of *Shearer* [1998] (using only cross-correlation data). We use a velocity model based on *Klein* [1981] and given in Table S1 of *Wolfe et al.* [2003]. The results of both methods are similar and the figures in this report show relocations using the method of *Waldhauser and Ellsworth* [2000]. The correlation pairs used are trimmed data that have removed large outliers (residuals > 50 ms) identified by the L1 norm grid search relative relocation. For the set of deep earthquakes, the final root-mean square error, with no further data downweighting, is 10 ms, indicating relative location accuracy on the order of 100 m. The relocation methods improve the relative locations between closely spaced earthquakes but velocity heterogeneity may still affect the relative locations between earthquakes spaced far apart. Hence long wavelength features, such as the exact dip of large fault zones, are not as accurately determined by hypocenter patterns.

4. Characteristics of Deep Earthquakes

[21] The relocation of all deep events is presented in Figure 8. The cross correlation data were able to relocate 7005 hypocenters, or 48% of the analyzed events. This calculation is a minimum estimate of the number of similar events, because pairs will not correlate highly if the signal-to-noise ratio is low: small magnitude events that are displaced far from stations, such as small, deeper earthquakes, are more difficult to constrain. Families of highly correlated earthquakes occur when there are closely spaced clusters with similar focal mechanisms, as at fault zones. Hence relocated clusters identify fault zones in the lithosphere beneath Hawaii. Our analyses relocated many clusters of earthquakes parallel to the southeast coast of Hawaii at depths of 25–50 km (Figure 8), indicating the existence of several tectonic fault zones in the mantle throughout this region.

[22] A plot of relocated earthquakes versus origin time reveals that most of these fault zones were

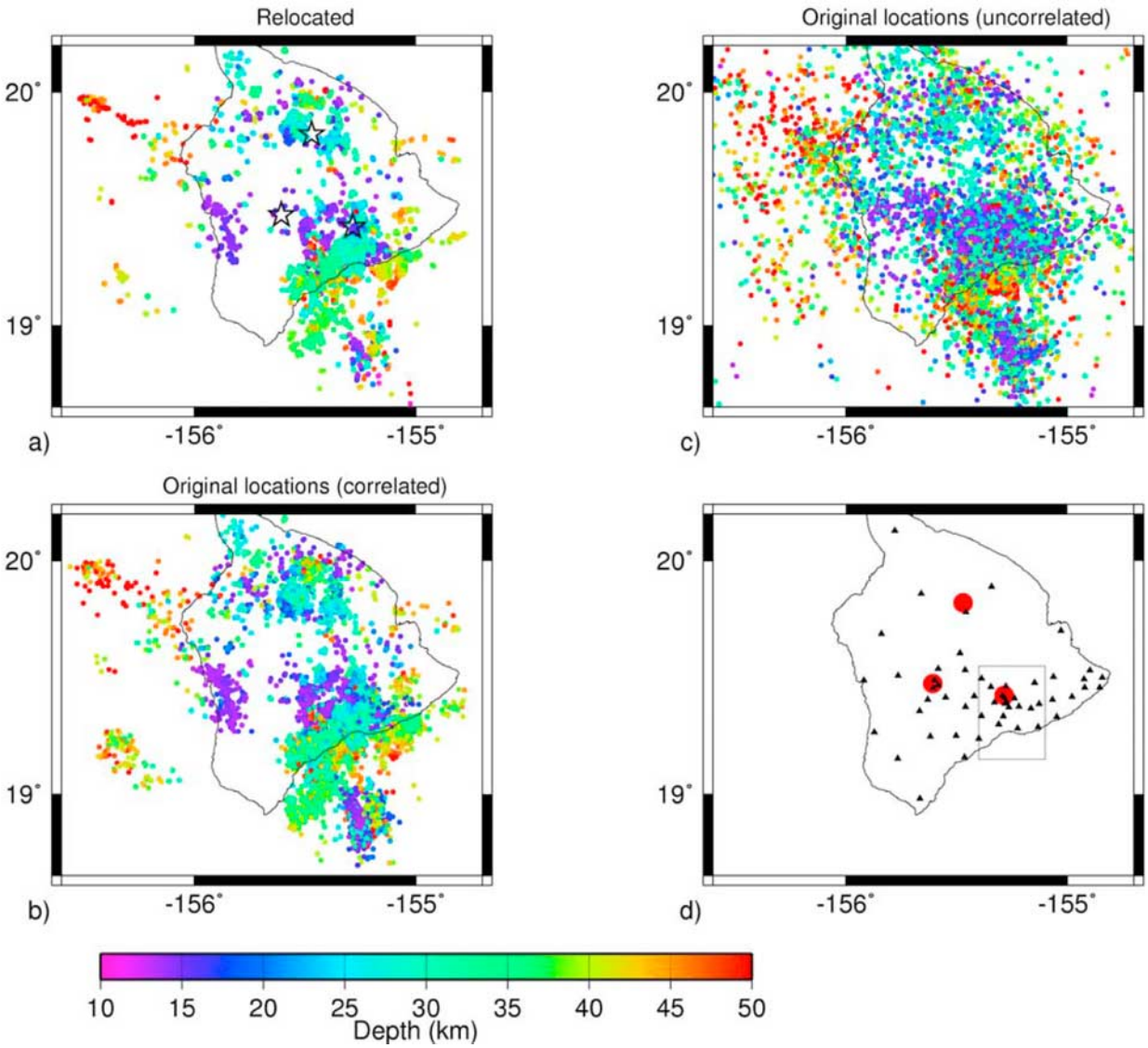

Figure 8. Map view of earthquakes (1988–1998) at Hawaii. (a) The 7005 relocated hypocenters derived using cross-correlation arrival time differences and the method of *Waldhauser and Ellsworth* [2000]. The locations of Kilauea, Mauna Loa, and Mauna Kea are indicated as stars. (b) Original catalog hypocenters for the subset of correlated earthquakes that were relocated. (c) Catalog hypocenters for the subset of 7599 earthquakes that did not correlate. d) Locations of stations (triangles) used in the relocation. The locations of Mauna Loa, Mauna Kea, and Kilauea are indicated by red circles and the box plots the region around Kilauea shown in previous and subsequent plots.

continuously active throughout the study period. The main exceptions where seismicity for a region was localized in time were the 1996 Loihi swarm [*Caplan-Auerbach and Duennebier*, 2001] and the aftershocks from three large offshore earthquakes in 1987 and 1988 (Figure 1b and Appendix). Because earthquakes in the 1996 Loihi swarm ranged mostly from 10–14 km depth, our data set includes only a subset of the Loihi earthquakes, of which 468 are associated in a multiplet based on the cross correlation linkages. Waveform modeling of an M_w 4.9 Loihi earthquake on 07/28/1996 yields a normal faulting solution (Figure 1b), which is consistent with first motion data for the 1996 Loihi swarm [*Caplan-Auerbach and Duennebier*, 2001]. Another small swarm of earthquakes occurred at Loihi in 2001, where in contrast two M_w 4.4 and 4.7 earthquakes have reverse

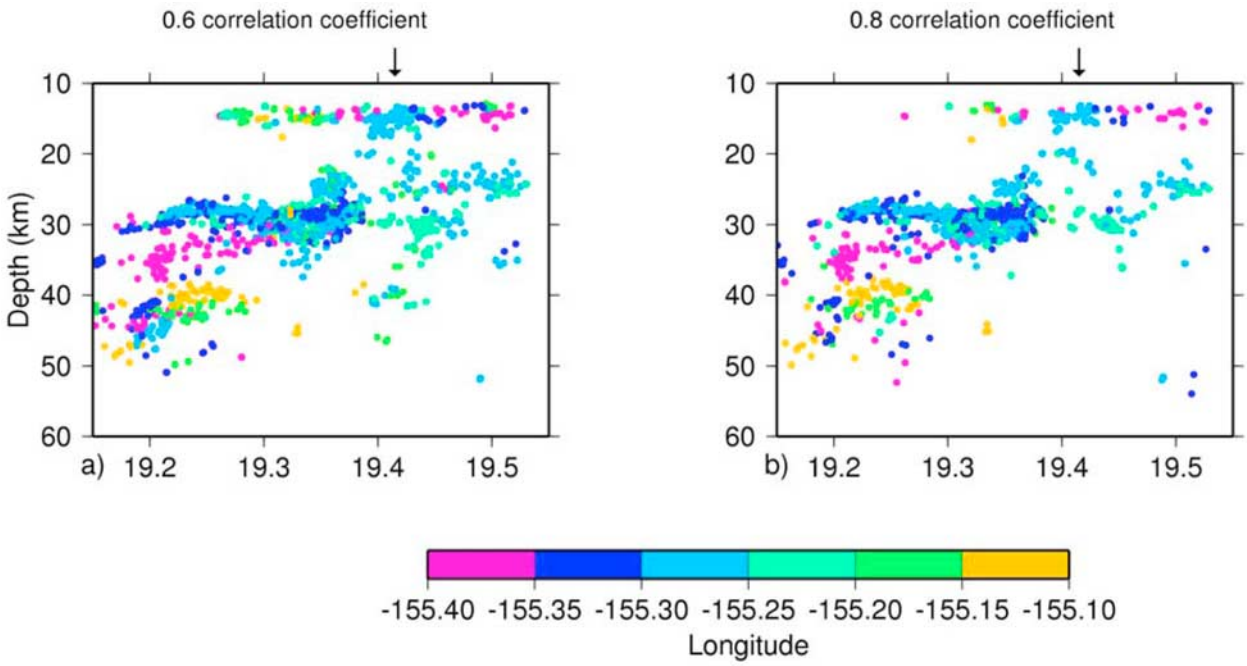

Figure 9. Vertical cross-sections of the region in Figure 3b. Earthquake locations are plotted as circles, with color indicating hypocenter longitude. (a) The 2522 relocated hypocenters derived using a cross correlation cutoff threshold of 0.6 and the method of *Waldhauser and Ellsworth* [2000]. The location of Kilauea caldera is indicated by a vertical arrow. (b) The 1636 relocated hypocenters using a cross correlation cutoff threshold of 0.8.

faulting mechanisms (Figure 1b). These different fault mechanisms between the 1996 and 2001 earthquake swarms suggest there may be differences in the underlying processes driving this seismic activity. On the basis of petrologic, geologic, and seismic data, *Caplan-Auerbach and Duennebier* [2001] suggest that the initial phase of earthquakes in the1996 swarm triggered drainage of a magma chamber, which lead to formation of a pit crater and caused a second phase of earthquakes in the swarm. Whereas the 1996 swarm may have reflected magma chamber drainage and normal faulting, it may be that the 2001 swarm with reverse faulting was associated with refilling of Loihi's summit magma chamber; a more definitive interpretation would, however, require higher precision constraints on the locations and depths of the earthquakes in these two swarms.

4.1. Earthquakes at Kilauea

[23] As described in *Wolfe et al.* [2003], one of the main features of the relocated seismicity at Kilauea is that a cluster of earthquakes near 30-km depth collapses to reveal a horizontally aligned fault zone (Figure 9a). This same pattern occurs if we relocate data using a high cross correlation cutoff of 0.8 (Figure 9b) and visualization of waveforms for the data in Figure 9a confirms the accuracy of the solutions (Figure 10). The distribution of relocated earthquakes also reveals several small, spatially distinct and unconnected fault zones, including ones that extend deeper offshore. There are few earthquakes relocated between 16–24 km depth. Below 16 km depth the events that we relocated do not suggest a magma conduit through the lithosphere, and such a feature also is not obvious in the patterns of the unrelocated earthquakes (see Figure 2c of *Wolfe et al.* [2003]).

[24] While 632 earthquakes (of which 335 are LP events) were relocated at depths shallower than 16 km, 2163 earthquakes located 13–20 km beneath Kilauea did not correlate and 1731 of these are LP events that may reflect magmatic processes. In a separate analysis of 2377 LP events, we used 21.5-s time windows (sliced −1.5 s before the predicted *P* wave arrival time), bandpass filtered the seismic data at 1–15 Hz, and applied a correlation threshold of 0.4. Analyses of the L1 norm

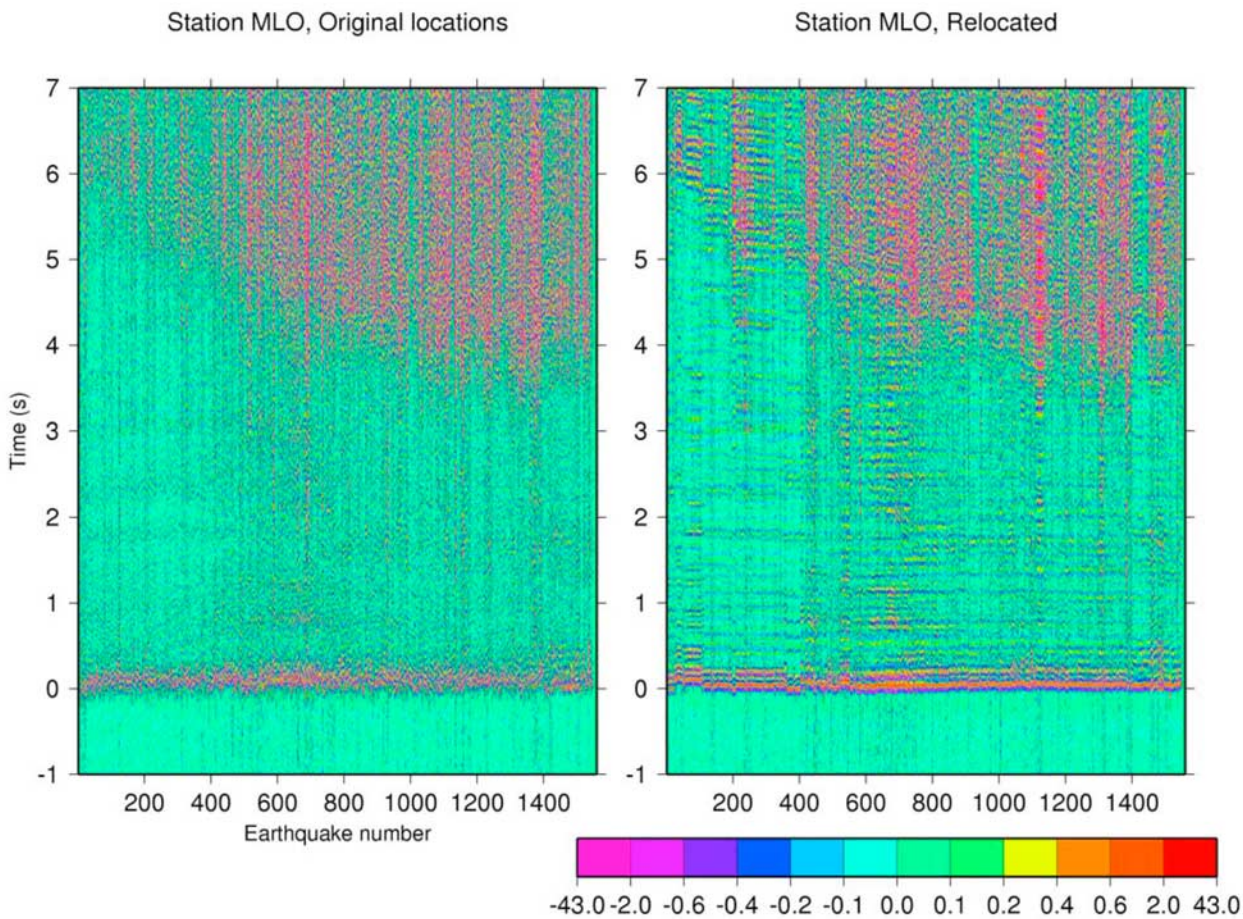

Figure 10. Waveforms for relocated earthquakes near 30 km depth (Figure 9a) at station MLO. Earthquakes are sorted by latitude. The x axis give the trace number and the color scale is proportional to the amplitude, which is normalized by the maximum amplitude in a −0.2–0.5 s window around the predicted *P* arrival. (a) Waveforms sliced around the predicted *P* wave arrival time using catalog parameters. (b) Waveforms sliced around the predicted *P* wave arrival time using relocated parameters. Notice that using the relocated parameters significantly sharpens the *P* wave arrival and its coda, although some small relative mislocation occurs in parts of the cluster.

unreconciled pair distance versus correlation coefficient reveals that although original distances for correlated pairs tend to span a few kilometers, the highest concentration of unreconciled relocated pairs is at distances less than 0.5 km apart. Using pairs with unreconciled pair distances less than 0.5 kilometer, we relocated 1256 LP events at Kilauea (Figure 11). In these relocations, a cylindrical cloud of seismicity at 13–20 km depth collapses to a more localized feature at 14–16 km depth. These relocations used a *P* wave velocity model, but we obtain a very similar pattern using an *S* wave velocity model. However, the seismic Moho in our velocity model is at 15.7 km depth, and we find that the maximum depth of this localized zone of earthquakes does correspondingly deepen when we employ a velocity model with a Moho at 18 km depth.

[25] We apply a cluster analysis using a joining algorithm [*Hartigan*, 1975] to the waveforms of relocated LP earthquakes, using the cross correlation coefficient between pairs of waveforms as a measure of similarity. This process orders waveforms so that similar waveforms will be placed closer together and dissimilar waveforms will be placed farther apart. Clustering (Figure 12) reveals that these LP earthquakes can be sorted into two sets with distinct waveforms. The first set (events ~1–372 in Figure 12b) has lower frequency wave-

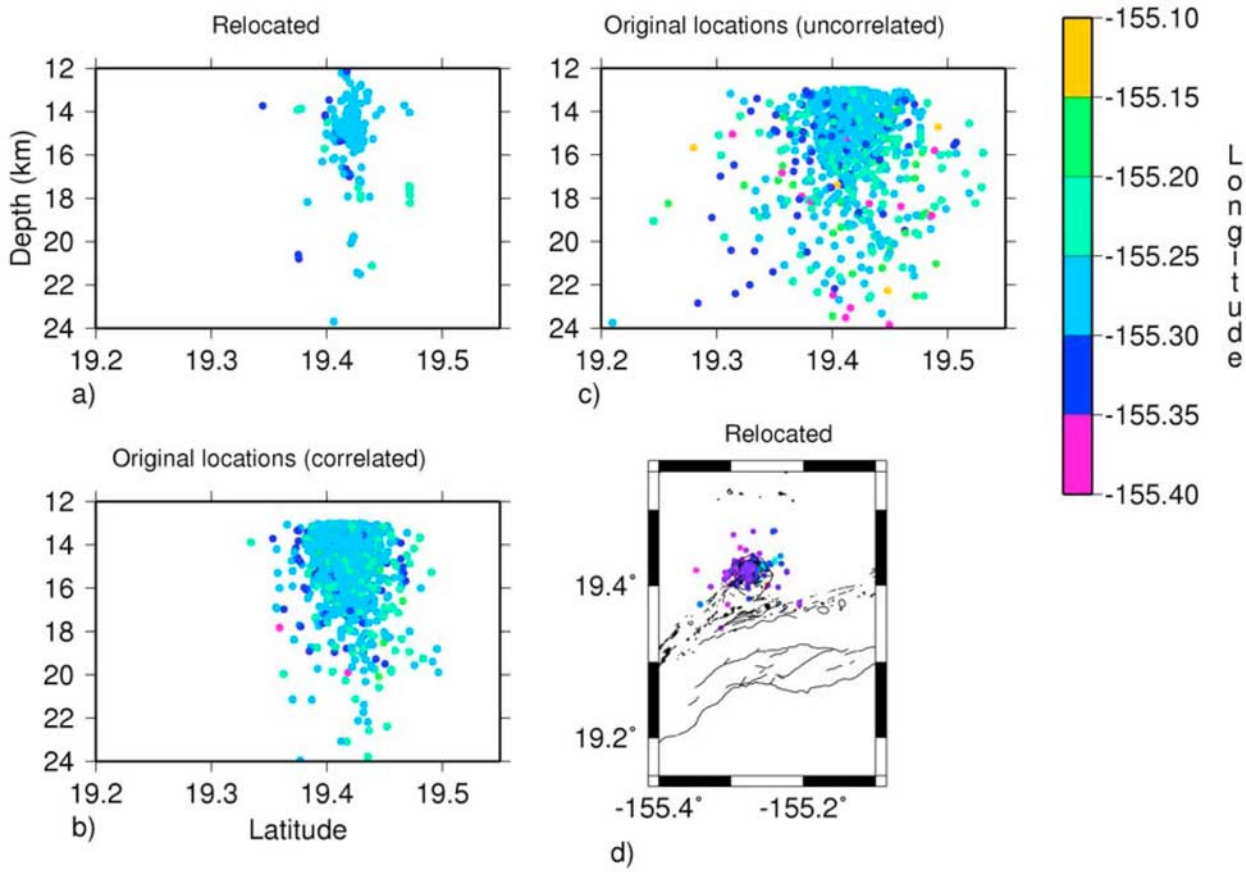

Figure 11. Vertical cross section of relocated LP earthquakes at Kilauea. (a) The 1256 relocated hypocenters derived using cross-correlation arrival time differences. (b) Original catalog hypocenters for the subset of correlated LP earthquakes that were relocated. (c) The 999 catalog hypocenters for the subset of LP earthquakes that did not correlate. (d) Map view of relocated LP earthquakes, with colors indicating depth according to the scale in Figure 9.

forms than the second set (events ~373–1271). The depths of the second set are localized (Figure 12a) near 15 km, whereas the depths of the first set are more diffuse and typically several hundred meters shallower than the first set. These patterns suggest that the LP earthquakes may occur from two nearly point-like sources, with one lower-frequency source located above a higher-frequency source. The larger spread in depths for the lower frequency source (Figure 12a) may reflect some remaining mislocation, as indicated by the diffuse *P* wave onsets in the waveform plot (Figure 12b). The lower frequency waveforms likely produce greater cross-correlation errors. At shallower depths beneath Kilauea, it has also been found that LP earthquakes with different spectral contents occur at different locations [*Almendros et al.*, 2002].

[26] The presence of a tectonic fault zone near 30-km depth is supported by the mechanisms of the earthquakes [*Wolfe et al.*, 2003]. Figure 13 shows the best double couple mechanism for the 1994 m_b 5.3 earthquake from the Harvard centroid moment tensor catalog [*Dziewonski et al*, 1994], which occurred at a depth of ~31 km (Table 1). For larger events (~m_L > 1.5), catalog travel time picks and phase polarities were available from 1974 to 2000. Composite mechanisms using FPFIT [*Reasenberg and Oppenheimer*, 1985] for earthquakes with catalog locations near the 30-km deep cluster (Figure 9) indicate that the dominant style of faulting is similar to the mechanism of the 1994 m_b 5.3 earthquake. The increase in the FPFIT misfit function as the earthquake magnitude decreases (Figure 13) likely indicates greater picking errors for smaller events and perhaps some true

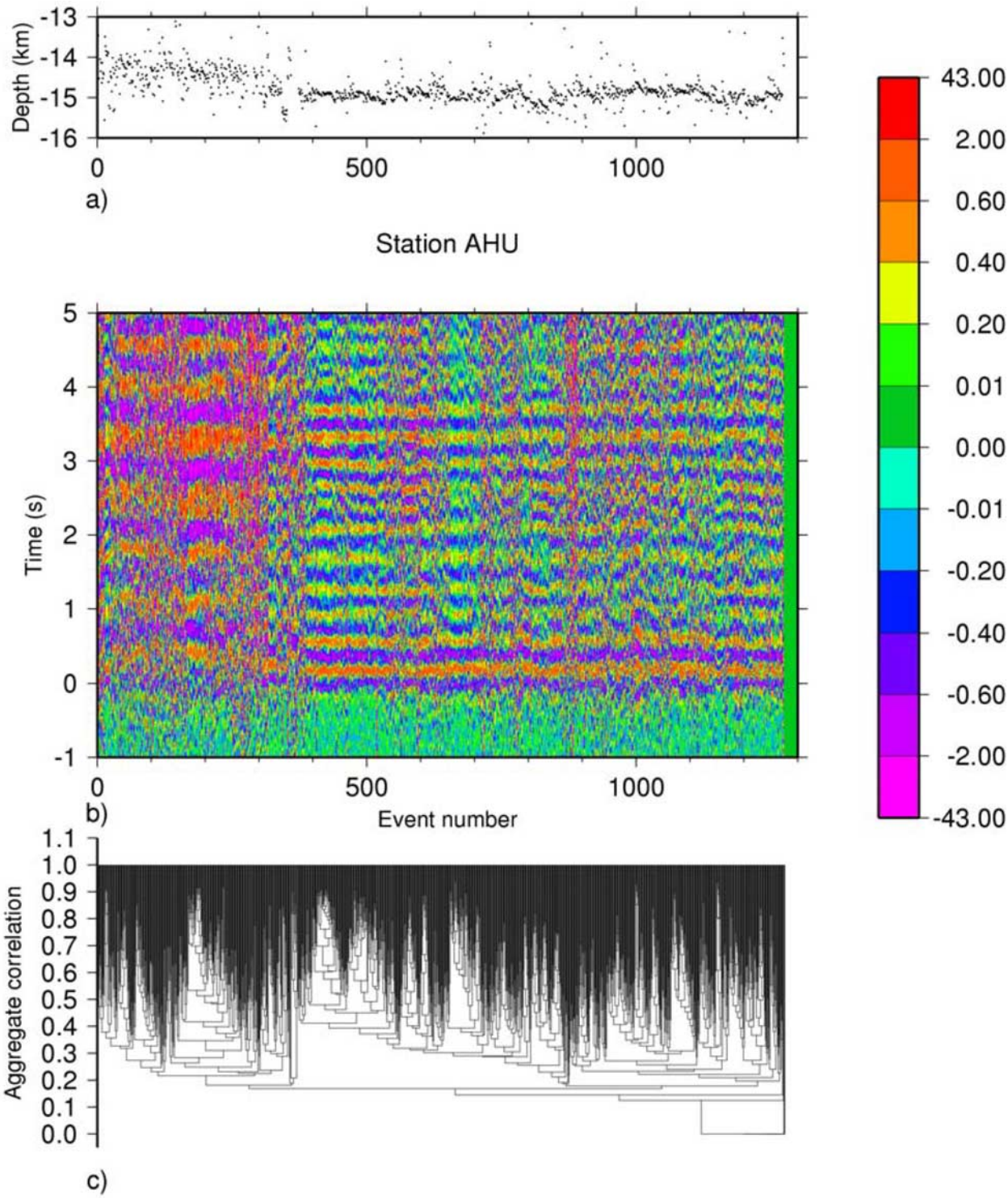

Figure 12. The characteristics of waveforms for relocated LP earthquakes (Figure 11a) at station AHU. The waveforms are ordered using a cluster analysis algorithm with the cross-correlation coefficient used as a measure of similarity. (a) Earthquake depth. (b) Waveforms sliced around the predicted *P* wave arrival time using relocated parameters. (c) Dendrogram for the data. A dendrogram is a hierarchical tree that describes how the objects are linked together and amalgamated into larger and larger clusters of increasingly dissimilar elements. The vertical axis denotes the linkage distance (aggregate correlation).

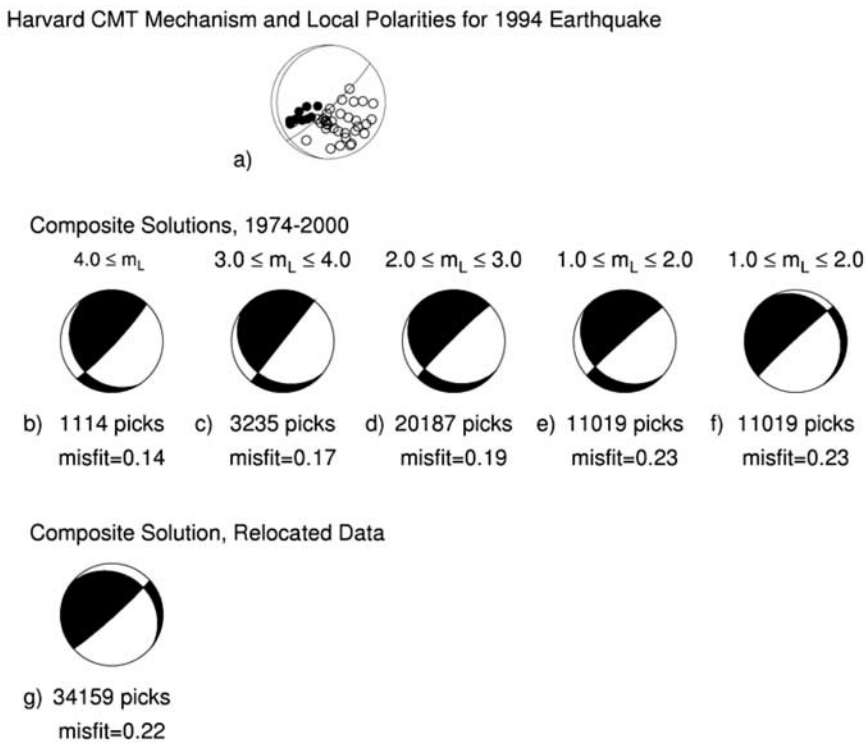

Figure 13. (a) Plot of first motion data for the 1994 m_b 5.3 earthquake, equal-area projection of the lower hemisphere. Solid circles are compressional arrivals; open circles are dilatational. Nodal plans of the best double couple solution from the Harvard centroid moment tensor catalog [*Dziewonski et al.*, 1994] are also shown. (b)–(f) Composite first motion solutions using FPFIT [*Reasenberg and Oppenheimer*, 1985] for four different magnitude intervals from the catalog of larger ($\sim m_L > 1.5$) earthquakes between 1974 and 2000 with catalog locations between 19.2°N to 19.4°N, 155.4°W to 155.1°W, and 20 to 40 km depth. The FPFIT misfit function (which is 0 for a perfect fit and 1 for complete misfit) and the number of polarities used in the composite solution are indicated. Two possible solutions are obtained for data with $1 \leq m_L \leq 2$. (g) Composite solution for relocated earthquakes (1988–1998, with no magnitude cutoff) near 30 km depth beneath Kilauea.

mechanism diversity at smaller magnitudes. The aftershocks of the 1994 m_b 5.3 earthquake make up a large proportion of the seismicity at 30-km depth between latitudes of 19.2°N to 19.3° at 155.3°W longitude, forming a north-south oriented line of epicenters. The pattern of aftershocks of the 1994 m_b 5.3 earthquake is therefore consistent with rupture being on the low-angle fault plane with seaward slip rather than on the northeast oriented vertical plane with oblique dip-slip motion. Catalog locations and magnitudes (Figures 2–4) further indicate the existence of a tectonic fault zone near 30-km depth that has been active for at least 40 years.

4.2. Earthquakes Throughout Hawaii

[27] In addition to the fault zone at Kilauea, our analyses relocated many clusters of earthquakes parallel to the southeast coast of Hawaii at depths of 25–50 km (Figures 8a and 14a), indicating the existence of several tectonic fault zones in the mantle throughout this region. Our analyses did not find correlated deep clusters of high frequency earthquakes at Mauna Loa volcano, which was not erupting during the time period 1988–1998 (but a small swarm of 15 LP earthquakes over 8 days beneath Mauna Loa was relocated near 30 km depth). However, several fault zones were found to the southeast of Mauna Loa at depths of 25–50 km (Figures 14a and 14b). Note that the large numbers of earthquakes near 19.4°N and 155.55°W at 13–15 km depth are part of the Kaoiki fault zone [c.f., *Jackson et al.*, 1992], which is located within the crust. Further study including shallower earthquakes in the analyses would be needed to more fully describe the earthquake characteristics at Kaoiki.

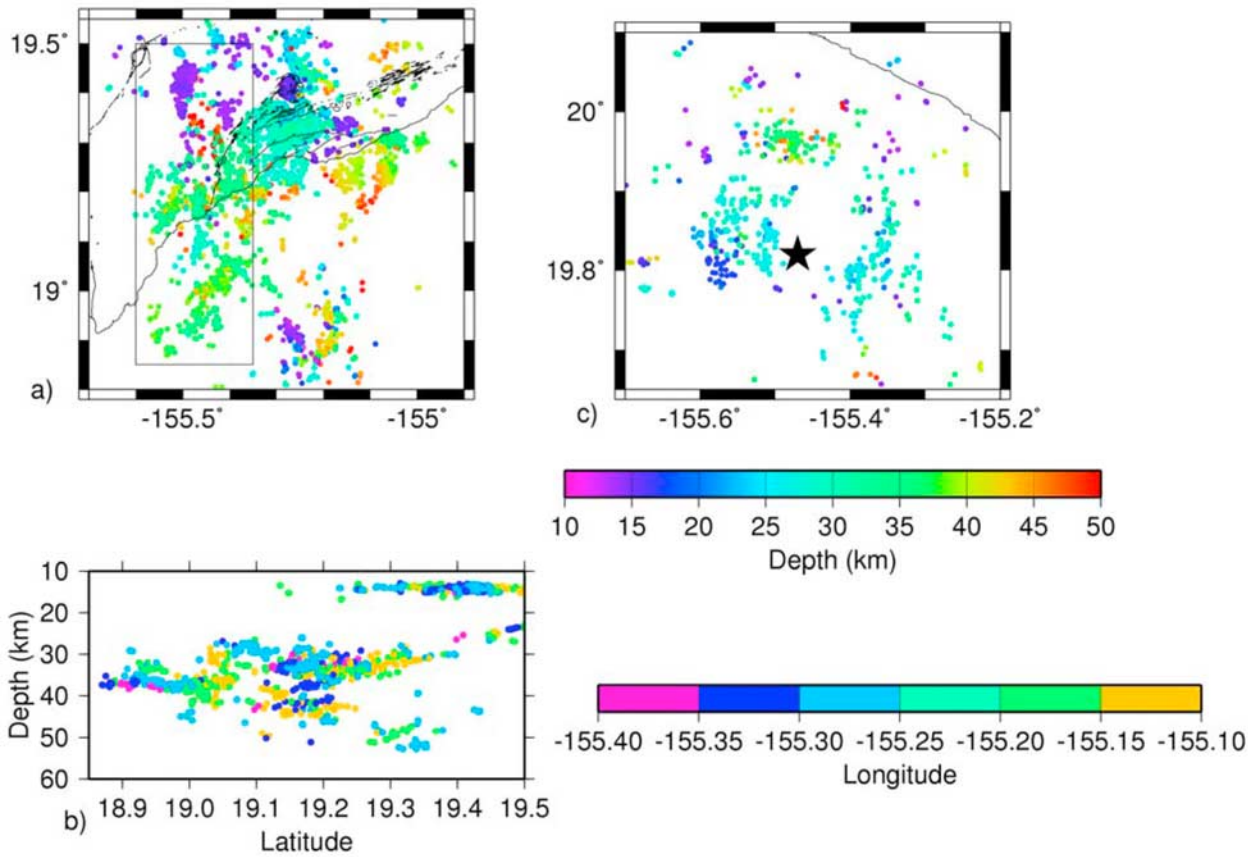

Figure 14. (a) Earthquakes relocated along the south flank of Hawaii. (b) Vertical cross sections of the boxed region in Figure 14a. (c) Earthquakes relocated at Mauna Kea. The location of the summit is denoted by a star.

[28] At Mauna Kea, we find that the relocated earthquakes at depths of 15–50 km form a ring around the summit (Figure 14c). Patterns of ring seismicity have been observed under other volcanoes, such as for earthquakes at 0–4 km depth at Rabaul caldera in Papua New Guinea [*Mori and McKee*, 1987] and earthquakes at mostly 7–14 km depth at Mount St. Helens [*Scandone and Malone*, 1985]. While shallow ring faulting at volcanoes may be associated with shallow magma-chamber processes [c.f., *Nettles and Ekström*, 1998], the cause of the deeper events at Mauna Kea is less clear.

[29] Because the mechanisms for individual earthquakes obtained from first motion polarities can be strongly affected by polarity picking errors, we instead calculate composite mechanisms for clusters of similar events using the FPFIT method [*Reasenberg and Oppenheimer*, 1985]. Composite mechanisms from similar event clusters yield more accurate focal mechanisms than can be obtained for individual events by reducing the effects of inconsistent polarity picks [c.f., *Shearer et al.*, 2003]. The HVO picked polarities are taken from the headers of the waveform data. The waveform cross-correlation linkages are used to associate earthquakes into clusters and the relocated hypocenters are used for calculating takeoff angle and azimuths. Only clusters with 5 or more earthquakes are examined. On the basis of visual inspection of the solutions, we discard poorly constrained mechanisms, where the solution misfit is high, the focal sphere coverage is inadequate, or the data patterns are ambiguous. Since several earthquakes in the southeast offshore region yielded similar results, we combine these clusters and obtain a single composite mechanism, although these offshore results should be considered more speculative due to the incomplete coverage. Figure 15 shows several examples of the data and solutions, which provide an indication of the quality of the mechanisms.

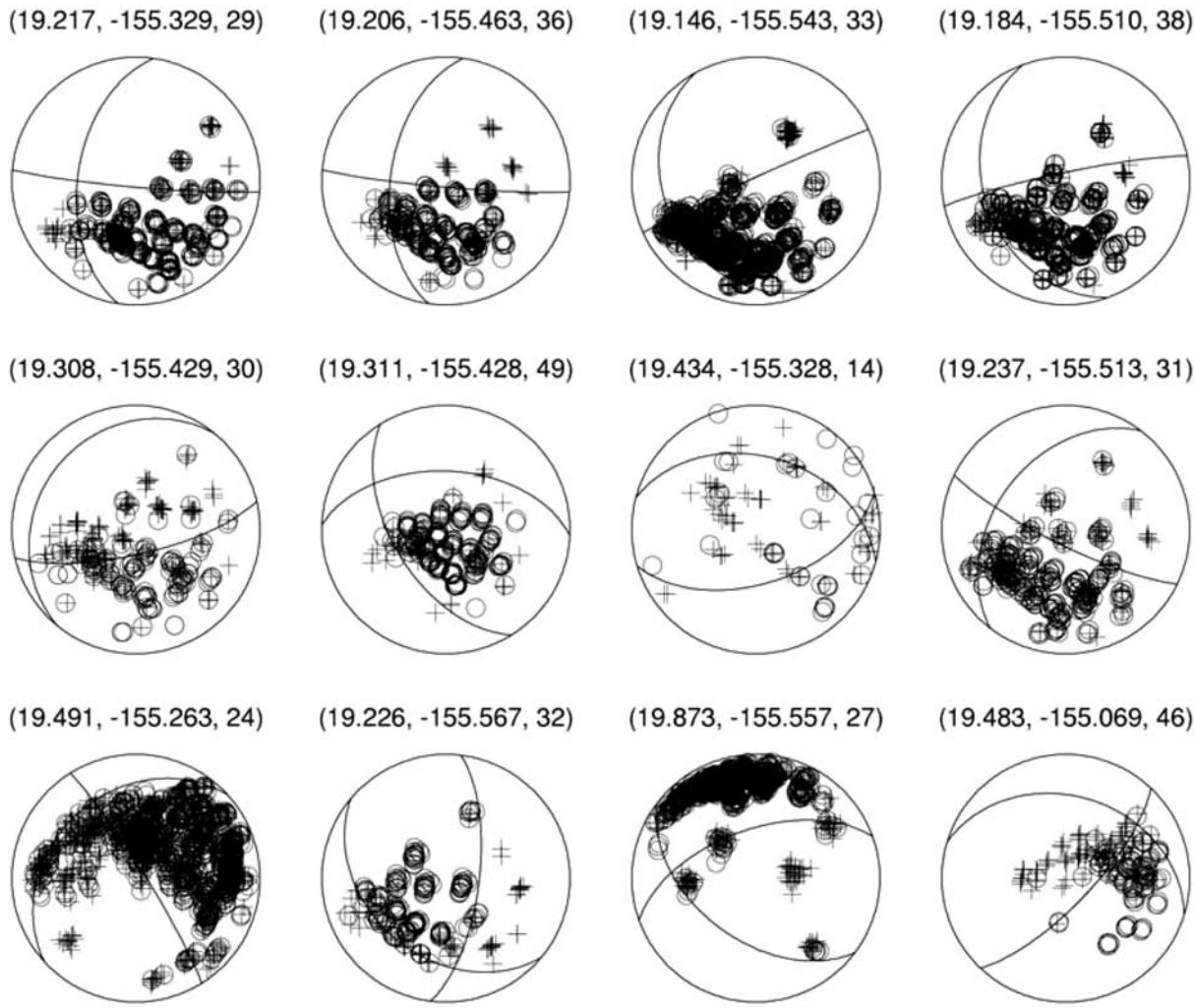

Figure 15. Example composite mechanism solutions for clusters of earthquakes, equal area lower-hemisphere projection. Dilatational polarity picks are plotted as open circles and compressional polarity picks are plotted as crosses. The nodal planes for the FPFIT solution mechanism are also shown. The average hypocenter for the cluster (latitude, longitude, and depth) is listed above the focal sphere.

[30] Figure 16 displays the composite mechanisms from this analysis as well as mechanisms from the analysis of earthquakes west of 155.55°W (see next section). The caption above each mechanism indicates the average depth of the cluster. Also plotted are the solutions from waveform modeling of several large earthquakes, such as the 1994 m_b 5.3 earthquake [*Dziewonski et al.*, 1994], the 1973 Honomu earthquake [*Unger et al.*, 1979; *Butler*, 1982; *Chen et al.*, 1990], and the m_b 5.5 earthquake in the west offshore region. Earthquakes in different depths and regions show consistent patterns of mechanisms. For instance, earthquakes near Mauna Kea at 26–32 km depth have reverse faulting mechanisms, most earthquakes at 26–41 km depth near the southeast coast have mechanisms similar to the 1994 m_b 5.3 earthquake (with one fault plane having seaward slip on a moderate to low-angle plane), and earthquakes northwest of Kilauea at 14 km depth have reverse faulting mechanisms. These consistent patterns suggest that several groups of fault zones may reflect similar underlying processes.

5. Earthquakes West of 155.55°W

[31] We relocate earthquakes west of 155.55°W by combining the deep waveform data with waveforms

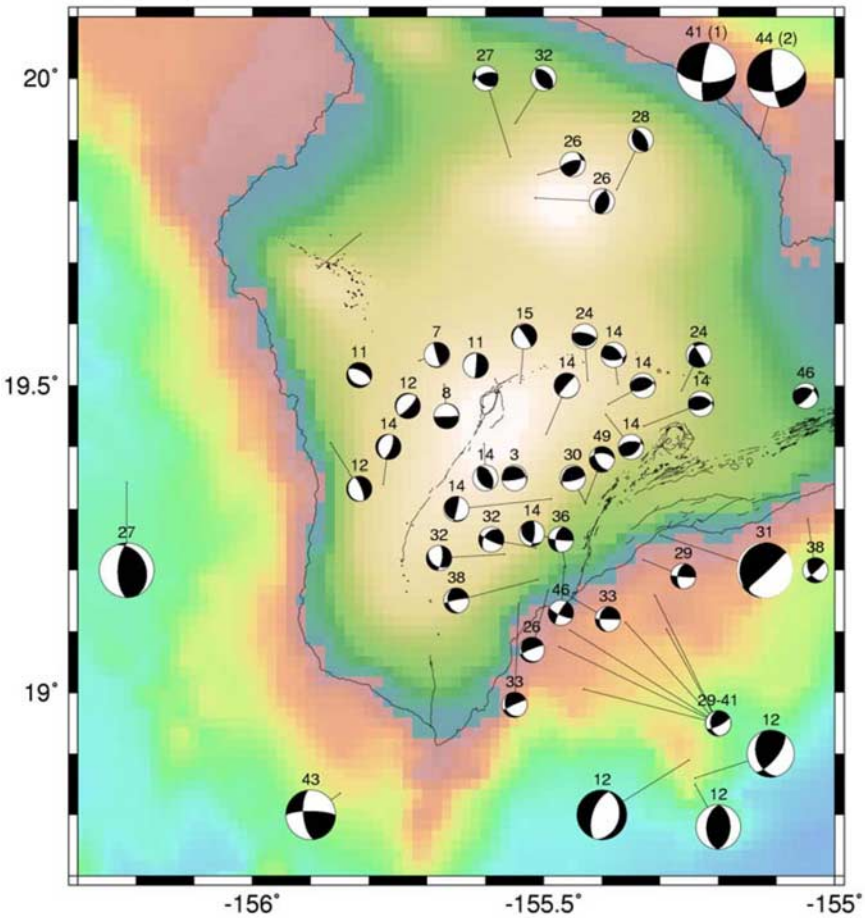

Figure 16. Map of composite mechanisms obtained at Hawaii. Earthquakes are sorted into clusters based on the linkages from waveform cross correlation, then composite mechanisms are obtained for each cluster. Only better-constrained mechanisms are plotted. The average depth of the cluster is indicated in the caption above each mechanism. We also plot the mechanisms and centroid depths of three large, deep earthquakes from waveform modeling. The mechanisms and depths for the 1973 Honomu earthquake, which was made up of two subevents, are from Wang-Ping Chen (personal communication, 2003), while the other large earthquakes are as in Figure 1b.

from 3963 shallow earthquakes west of 155.55°W recorded from 1988–March 1998. The combined data set yields waveforms for 6673 earthquakes west of 155.55°W. We apply the cross correlation and relocation methods discussed in section 3 to this data set. Unlike the case for deep earthquakes (Figure 7), most earthquake pairs obtained using a cross-correlation threshold of 0.6 have unreconciled relocated pair distances of 2.5 km or less (Figure 17). The correlation coefficient between earthquake pairs likely depends on a number of factors, including ray path geometry, station distances, focal mechanisms, earthquake magnitudes, and the scattering properties of the medium. The different patterns in correlation coefficient versus pair distance for the two data sets (Figures 7 and 17) may occur because for deeper earthquakes the takeoff angle to nearby stations changes more slowly with location than for shallow earthquakes, thereby affecting how rapidly the seismic radiation pattern changes with pair distance.

[32] We are able to relocate 3623 earthquakes using a cross-correlation threshold of 0.6; the results are similar whether or not we use a filtered subset of event pairs, which only includes a pair if its L1-norm, grid search, unreconciled relative locations from the cross-correlation data are less than 2 km apart. Figure 18 displays the results of relocation. The boxed region in Figure 18 indicates

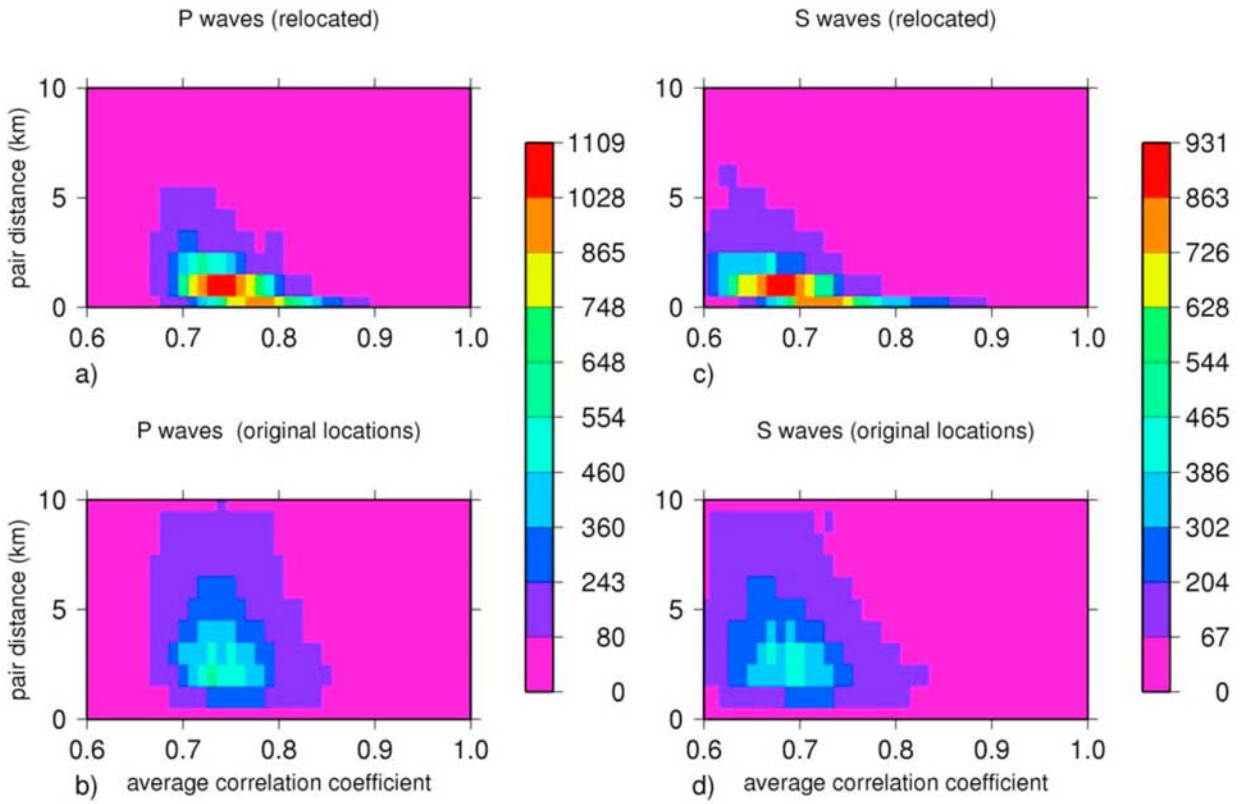

Figure 17. Plots of the pair distance versus the average cross correlation coefficient of the data for earthquakes west of 155.55°W. A cross correlation threshold of 0.6 is used. See Figure 7 for further information.

the Kealakekua fault zone [c.f., *Gillard et al.*, 1992], where we find that a high percentage of earthquakes correlate and can be relocated. Notice that few earthquakes occur on Mauna Loa's west flank south of 19.2°N; *Wyss and Koyanagi* [1992b], have suggested that this south Kona gap is a region of strain accumulation and could be a likely place for a future large earthquake, but alternatively slip could be aseismic in this region.

[33] Figure 19 displays a vertical cross section of earthquake longitude versus depth for the region around the Kealakekua fault zone. The original locations in this region show a large spread in depth (Figure 19b), but upon relocation, the hypocenters become more localized in depth (Figure 19a). The pattern of seismicity is consistent with the suggestion that, like the south flank of Hawaii, the Kealakekua fault zone reflects an inland-dipping low-angle detachment. In accordance with this hypothesis, composite mechanisms from clusters of similar relocated earthquakes in west Hawaii generally yield a solution with one fault plane having seaward slip on a low-angle plane (Figure 16).

[34] Some clusters of correlated earthquakes, indicating fault zones, are located in the region offshore of west Hawaii. There are several correlated earthquakes near 19.2°N, 156.4°W, and 40 km depth. This region experienced an m_b 5.5 earthquake in 1991, but the relocated earthquakes are not all immediate aftershocks of this earthquake. Instead they are spread throughout the study

Figure 18. Map view of earthquakes analyzed at west Hawaii. (a) The 3623 relocated hypocenters derived using cross-correlation arrival time differences. Box denotes region is plotted in Figure 18d. (b) Original catalog hypocenters for the subset of correlated earthquakes that were relocated. (c) The 3051 catalog hypocenters for the subset of earthquakes that did not correlate. (d) Relocated hypocenters in the Kealakekua region.

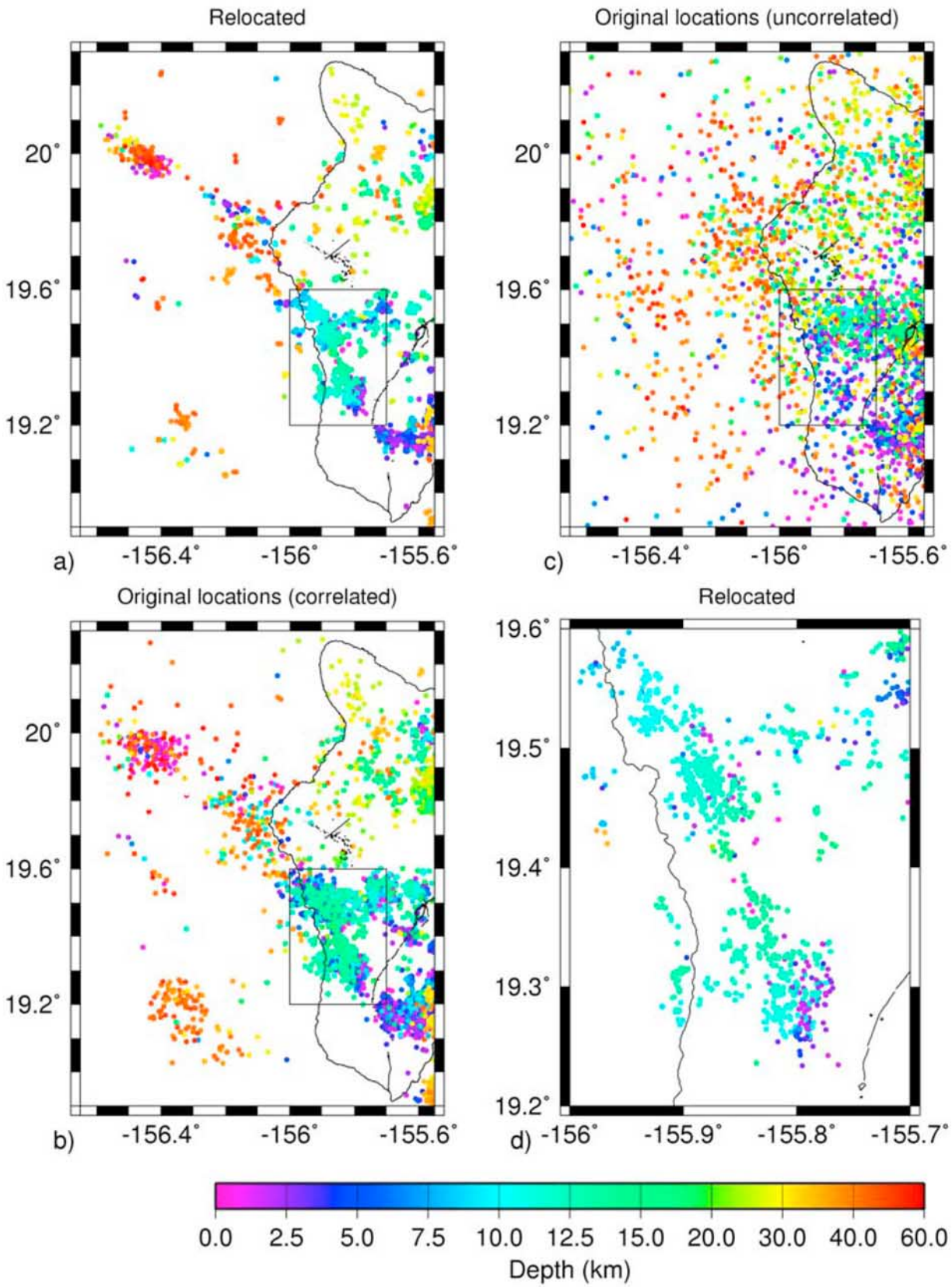
Relocated
Original locations (uncorrelated)
Original locations (correlated)
Relocated
20°
19.6°
19.2°
19.5°
19.4°
19.3°
-156.4°
-156°
-155.6°
-155.9°
-155.8°
-155.7°
a)
b)
c)
d)
0.0
2.5
5.0
7.5
10.0
12.5
15.0
20.0
30.0
40.0
60.0
Depth (km)

Figure 18.

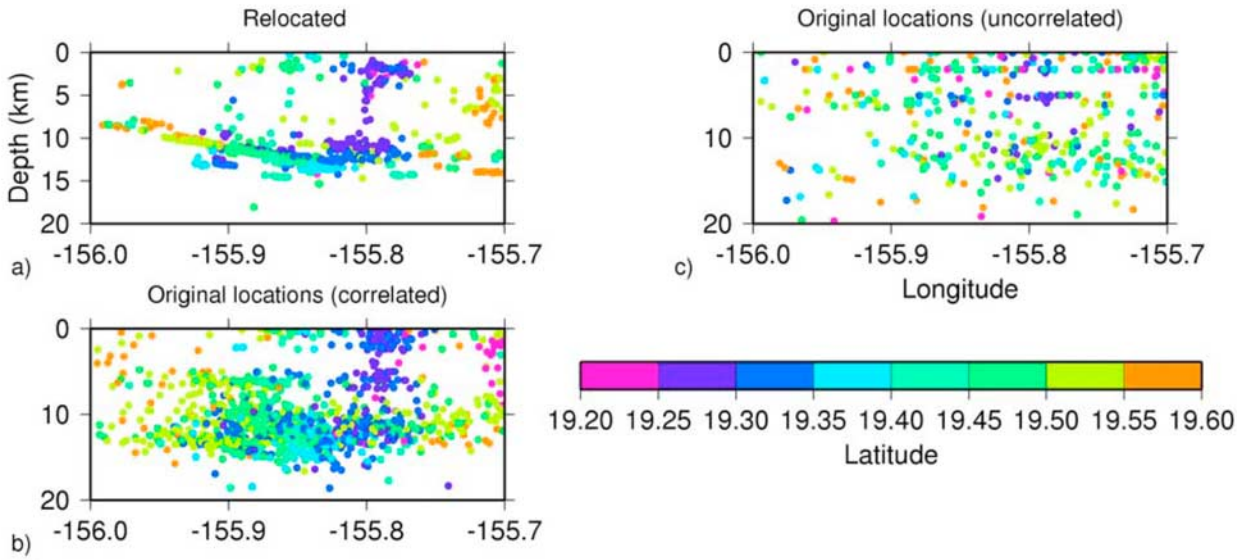

Figure 19. Vertical cross-sections of the region in Figure 18d. Earthquake locations are plotted as circles, with color indicating hypocenter latitude. (a) The 1084 relocated hypocenters. (b) Original catalog hypocenters for the subset of correlated earthquakes that were relocated. (c) The 507 catalog hypocenters for the subset of earthquakes that did not correlate.

period, indicating a continuously active fault zone. CMT modeling of the m_b 5.5 earthquake yields a depth of 26.9 km and modeling of teleseismic *P* waves [*Ekström*, 1989] also supports a depth near 28 km (Table 1).

[35] In contrast, most offshore earthquakes near 19.9°N, 156.4°W occurred in 1988 and are likely aftershocks of the three large offshore earthquakes that occurred in 1987 and 1988 (Figure 1b). The HVO catalog depths of earthquakes in this area are bimodal, with some being shallow (mostly 0 km depth) and others being deep (mostly 40–60 km depth). To test whether these earthquakes could be in a single cluster at a similar depth, we cross correlate all earthquakes in this region without a distance cutoff. Figure 20 shows the RMS of the unreconciled L1 norm grid search relocations versus either relocated pair distance (Figure 20a) or the original pair distance (Figure 20b); relocation of correlated event pairs removes the bimodal spread in pair distances, indicating that these earthquakes originate at a common depth. Full relocation using the method of *Shearer* [1998] also removes the bimodal depth character, but relocations of the cluster using the method of *Waldhauser and Ellsworth* [2000] require several hundred iterations to move these earthquakes close together, which may be due to the large mislocations in the initial hypocenters and the weak depth resolution of these data. Thus it appears that the spread in depths in the initial locations is an artifact of these events being far outside of the HVO seismic network, where depths can be poorly constrained. Although these high precision relocations do not place good constraints on the absolute depth of the cluster [c.f., *Wolfe*, 2002], teleseismic *P* wave modeling using the method of *Ekström* [1989] yields depths of 9.5 and 9.6 km for the earthquakes of 02/04/1987 and 03/28/1988 (Table 1) and a shallow depth is also obtained for the earthquake of 03/25/1988 (Table A1). These three shallower earthquakes may occur on faults that are somehow related to the offshore rift zones of Hualalai or Kohala volcanoes, or with Mahukona volcano. The 02/21/1976 earthquake (Figure 1b) may also be associated with these offshore features and the 04/26/1986 earthquake could be associated with the Hana ridge, which is Haleakala's submarine east rift zone.

6. Discussion

[36] The cross-correlation relocation and focal mechanisms of deep earthquakes throughout

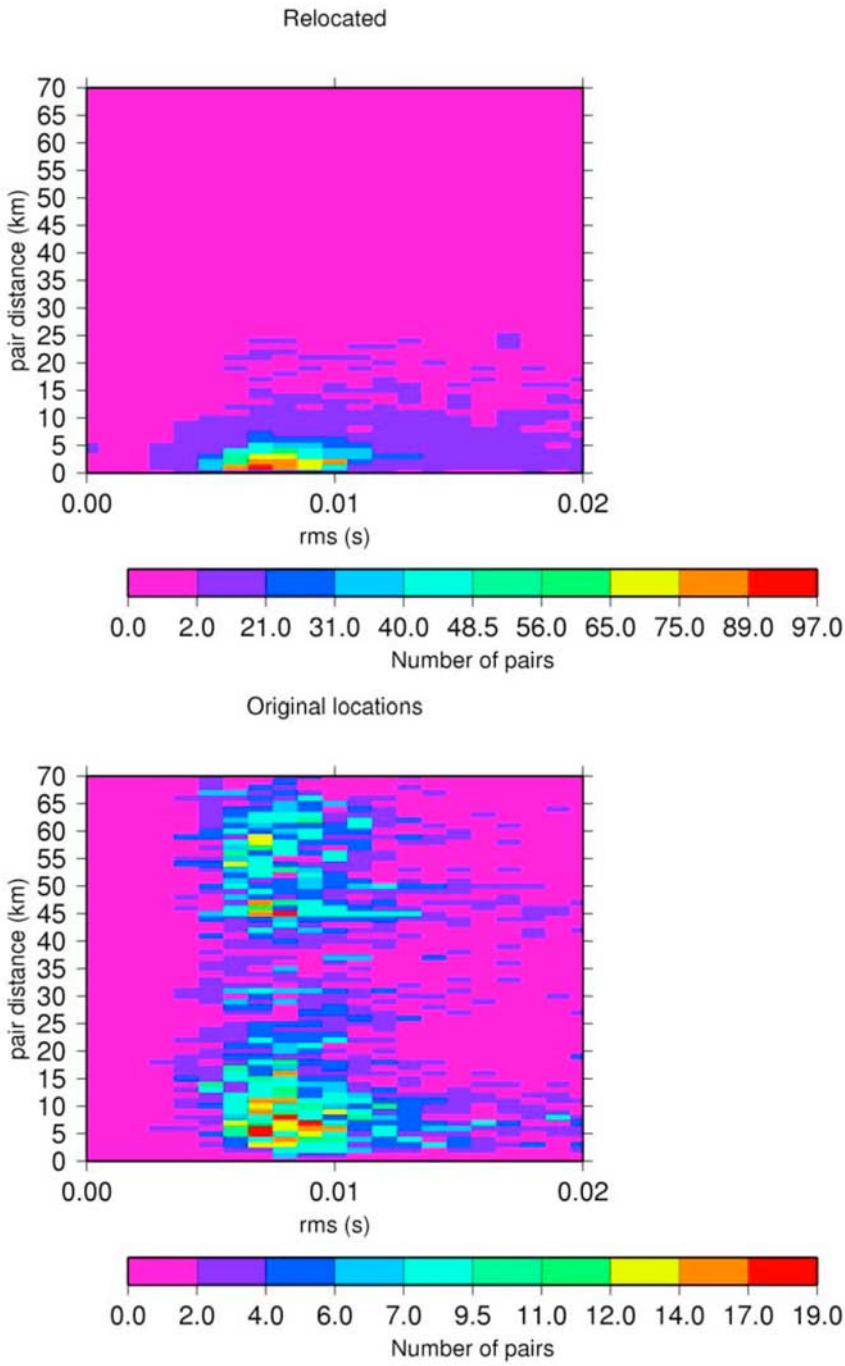

Figure 20. Plots of pair distance versus RMS error for L1 norm unreconciled solutions for a subset of earthquakes near 19.9°N, 156.4°W. No distance cutoff was used in the cross correlations. (a) L1 norm unreconciled relocations are used to calculate pair distance. (b) Original locations are used to calculate pair distance.

Hawaii provide evidence of abundant tectonic fault zones in the lower crust and upper mantle. At Kilauea, it has been suggested [*Eaton and Murata*, 1960; *Klein et al.*, 1987; *Ryan*, 1988; *Tilling and Dvorak*, 1993] that earthquakes outline a pipe-like magma conduit that extends through the lithosphere to depths as great as 60 km, thereby delineating the magma pathway from its source to the surface. The LP earthquakes at 14–16 km depth (Figure 11), which are likely generated at

Table A1. Earthquake Parameters[a]

Date	Time, UT	Lat.	Lon.	Depth, km	Strike	Dip	Rake	Strike	Dip	Rake	M_0 dyne-cm	M_W, dyne-cm
1976/02/21	05:51	20.18	−156.11	12.0	98°	66°	−164°	1°	76°	−25°	1.9×10^{23}	4.8
1986/04/26	17:19	20.76	−155.56	12.1	229°	65°	165°	326°	77°	26°	7.1×10^{23}	5.2
1988/03/25	00:29	19.85	−156.44	12.0	264°	42°	23°	156°	75°	129°	6.2×10^{23}	5.1
1991/05/08	18:21	19.34	−156.08	27.6[b]	336°	29°	67°	182°	63°	102°	1.8×10^{24}	5.4
1991/12/09	23:14	18.67	−155.96	43.5	174°	65°	166°	270°	77°	26°	2.5×10^{23}	4.9
1996/07/28	09:30	18.70	−155.23	12.0	12°	31°	−96°	199°	59°	−86°	2.8×10^{23}	4.9
2001/09/11[c]	00:09	18.51	−154.97	12.0	182°	45°	90°	2°	45°	90°	4.2×10^{22}	4.4
2001/09/13	13:11	18.60	−154.92	12.0	161°	38°	39°	38°	67°	121°	1.3×10^{23}	4.7

[a] Date and time are from the NEIC catalog; locations are those determined in this study.
[b] Depth determined by very-broad-band analysis of *P* waveforms.
[c] Vertical dip-slip components of the moment tensor were constrained to zero.

two point sources (Figure 12), may reflect resonance of sections of a fluid-filled magma conduit. On the basis of constraints from seismic and gravity data [*Hill and Zucca*, 1987], these relocated shallower LP earthquakes could occur just above the base of the crust at Kilauea.

[37] However, below about 16 km depth, our study demonstrates that many high-frequency earthquakes near Kilauea are focused on an active fault zone at 30-km depth, with seaward slip on a low-angle plane, and other smaller, distinct fault zones. These earthquakes predominantly reflect tectonic faulting in the brittle lithosphere rather than magma movement associated with volcanic activity. The association of this highly active and long-lived seismic zone (Figure 2) with the frequently erupting Kilauea volcano implies that the tectonic faulting may be triggered by stresses of magmatic origin, although the background stresses from volcano loading and flexure may help bring faults close to failure. In a study of the 1983 dike intrusion at Kilauea [*Rubin et al.*, 1998], earthquake characteristics indicated that the intrusion may have induced seismicity on preexisting faults in regions of significant ambient (i.e., preintrusion) differential stress. Elastic stress modeling is also consistent with the idea that dike-induced seismicity reflects the distribution of ambient stresses that are near to failure and does not necessarily reflect the extent of the dike [*Rubin and Gillard*, 1998]. Analogously, the highly active 30-km deep fault zone beneath Kilauea may reflect magma-induced seismicity on preexisting faults in a region of significant ambient stresses from volcano loading and flexure.

[38] For earthquakes below 23 km depth near the coast of Hawaii, both onshore and offshore, many mechanisms have one fault plane exhibiting low-angle or moderate dip and seaward (coast perpendicular) slip of the hanging wall (Figure 16). These mechanisms may be consistent with the patterns of stresses predicted from some finite element models of volcano loading and plate flexure for Tharsis volcano on Mars [*McGovern and Solomon*, 1993]. In such models, at some depths in the lithosphere near the edges of a sloping volcano, the maximum compressive stress is inclined from vertical and is directed radially outward (i.e., having components both downward and radially outward) and the minimum principal stress is also in the radial plane. This type of stress field would produce seaward (coast normal) slip on preexisting faults, as generally observed around Hawaii's perimeter at depths of ~24–41 km (Figure 16). For some of these models, at greater depths near the perimeter of the volcano, the maximum principal stress is near horizontal and radial and the minimum principal stress is out of the radial plane (i.e., circumferential), which would be consistent with the oblique strike-slip mechanism of the 1973 41–44 km deep Honomu earthquake and the strike-slip 43 km deep earthquake of 12/09/1991. Directly beneath the volcano center, the models of *McGovern and Solomon* [1993] predict at shallow depths that the maximum principal stress is horizontal and radial and the minimum principal stress is vertical. This stress field could produce the reverse faulting

earthquakes seen under Mauna Kea. At deeper depths directly beneath the volcano center, the maximum principal stress becomes vertical and the minimum compressive stress becomes horizontal and radial, which would produce normal faulting.

[39] Thus a comparison of pattern of mechanisms with the stresses predicted from finite element models suggests that deep earthquakes at Hawaii may reflect ambient stresses from volcano loading and flexure acting on preexisting faults, although further finite element modeling work specific to Hawaii is needed to better assess this hypothesis. It is also not clear whether the several reverse faults northwest of Kilauea at 14 km depth are due to the effects of volcano loading and flexure or are due to the buttressing of the growing Kilauea volcano by Mauna Loa.

[40] Both the focal mechanism analyses (Figure 16) and the patterns of relocated seismicity at the Kealakekua fault zone (Figure 19) are consistent with the hypothesis that there is an inland-dipping low-angle detachment fault beneath the west flank of Mauna Loa with seaward slip that likely occurs at the boundary of the volcano edifice and the oceanic crust [*Gillard et al.*, 1992; *Wyss and Koyanagi*, 1992b; *Beiser et al.*, 1994]. Since 1950, Mauna Loa has erupted only twice, so the earthquake activity on the Kealakekua fault zone recorded by the modern HVO seismic network may presently have lower moment rates than in previous times. The moment rate may correspondingly increase if Mauna Loa experiences increased volcanic activity and rift zone expansion, which would drive faulting on the detachment. Indeed, the magnitude 6.9 Kona earthquake occurred in 1951 following the period from 1832 to 1950 when Mauna Loa erupted once every 3.4 years on average.

7. Conclusion

[41] The relocations, waveform, and focal mechanism analyses for earthquakes in Hawaii presented in this paper provide a new view of tectonic processes and improve our understanding of the causes of earthquake hazards in regions away from the southeast flank. Cross-correlation relocation of deep earthquakes provides evidence of many tectonic fault zones in the lower crust and upper mantle, and the characteristics of deep earthquakes are consistent with stresses from volcano loading and flexure acting on preexisting faults. At Kilauea, the stresses from magma movement may additionally help trigger mantle earthquakes on preexisting faults in regions with high differential ambient stresses. Long-period earthquakes at ~14–16 km depth beneath Kilauea could indicate resonance of two portions of a magma conduit in the lower crust. At the Kealakekua fault zone, the patterns of relocated seismicity and focal mechanisms are consistent with the existence of a seismically active detachment between the volcano edifice and the oceanic crust.

Appendix A: Determination of CMT Solutions

[42] This study presents centroid-moment-tensor solutions for eight earthquakes of moment magnitude M_w = 4.4–5.4 (Figure 1 and Table A1). These events were too small for analysis using the standard Harvard CMT approach [*Dziewonski et al.*, 1981; *Dziewonski and Woodhouse*, 1983], which, for earthquakes smaller than $M_w \sim 6$ relies on fitting long-period ($T > 45$ s) body waves. Here, we use a modified version of the CMT algorithm [*Arvidsson and Ekström*, 1998; *Ekström et al.*, 1998] that fits first-arriving surface waves at intermediate periods (35 s < T < 150 s). The excitation of the surface waves is calculated using the appropriate, local crustal structure at the earthquake hypocenter, as given by *Bassin et al.* [2000] and *Mooney et al.* [1998]. Dispersion of the surface waves between the source and receiver is then predicted using the phase-velocity maps of *Ekström et al.* [1997]. For the one event we analyze in 1976, stations of the High-Gain Long-Period (HGLP) network are included using the response information determined by *Ekström and Nettles* [1997]. Use of the intermediate-period surface waves greatly increases the signal-to-noise ratio for small (M_w < 5.5) earthquakes like those considered here.

[43] We attempted surface-wave CMT analyses for events in the region between 18°–21°N and

154°–157°W for which the National Earthquake Information Center (NEIC) listed a magnitude M > 5.0, and for which the Harvard CMT catalog does not contain a solution. We excluded events in the Kilauea region, as numerous solutions for larger events in this area can be found in the CMT catalog. We also attempted solutions for several smaller (M < 5.0) earthquakes near Loihi seamount. Of the 13 events considered, five were too small or too noisy for successful analysis. Results for the eight events successfully analyzed are presented in Figure 1 and Table A1; the complete source parameters in the standard Harvard CMT electronic format are available from the authors. We do not consider the centroid locations determined here to provide better locations for these events than the hypocenters determined by HVO and the NEIC, though in several cases we were able to improve on reported standard depths (0 or 33 km). The depths of shallow events were constrained to remain greater than or equal to 12 km in our analysis, to prevent instabilities in the retrieval of the vertical dip-slip components of the moment tensor that can occur at shallower depths.

Acknowledgments

[44] This research was supported by NSF under grant EAR-0106357. We thank Garrett Ito, Patrick McGovern, Gary Pavlis, and Paul Wessel for discussions. Greg Beroza, Allan Rubin, Jean-Luc Got, and Karen Fischer provided constructive comments in the review process that improved the paper. This is SOEST contribution number 6359 and HIGP contribution number 1322.

References

Aki, K., and R. Koyanagi (1981), Deep volcanic tremor and magma ascent mechanism under Kilauea, Hawaii, *J. Geophys. Res.*, *86*, 7095–7109.

Almendros, J., B. Chouet, P. Dawson, and T. Bond (2002), Identifying elements of the plumbing system beneath Kilauea volcano, Hawaii, from the source locations of very-long-period signals, *Geophys. J. Int.*, *148*, 303–312.

Arvidsson, R., and G. Ekström (1998), Global CMT analysis of moderate earthquakes, Mw > 4.5, using intermediate period surface waves, *Bull. Seismol. Soc. Am.*, *88*, 1003–1013.

Bassin, C., G. Laske, and G. Masters (2000), The current limits of resolution for surface wave tomography in North America, *Eos Trans. AGU*, *81*(48), Fall Meet. Suppl., Abstract S12A-03.

Beiser, M., D. Gillard, and M. Wyss (1994), Inversion for source parameters from sparse data sets: Test of the method and application to the 1951 (M = 6.9) Kona, Hawaii, earthquake, *J. Geophys. Res.*, *99*, 19,661–19,678.

Bergmanis, E. C., J. M. Sinton, and F. A. Trusdell (2000), Rejuvenated volcanism along the southwest rift zone, East Maui, Hawaii, *Bull. Volcanol.*, *62*, 239–255.

Butler, R. (1982), The 1973 Hawaii earthquake: A double earthquake beneath the volcano Mauna Kea, *Geophys. J. R. Astron. Soc.*, *69*, 173–186.

Caplan-Auerbach, J., and F. K. Duennebier (2001), Seismicity and velocity structure of Loihi Seamount from the 1996 earthquake swarm, *Bull. Seismol. Soc. Am.*, *91*, 178–190.

Chen, W.-P., J. Nábelek, and M. A. Glennon (1990), Source parameters of the June 26, 1989 Hawaiian earthquake (abstract), *Eos Trans. AGU*, *71*, 562.

Chouet, B. (1996), Long-period volcano seismicity; its source and use in eruption forecasting, *Nature*, *380*, 309–316.

Delaney, P. T., R. S. Fiske, A. Miklius, A. T. Okamura, and M. K. Sako (1990), Deep magma body beneath the summit and rift zones of Kilauea Volcano, Hawaii, *Science*, *247*, 1311–1316.

Denlinger, R. P., and P. G. Okubo (1995), Structure of the mobile south flank of Kilauea Volcano, Hawaii, *J. Geophys. Res.*, *100*, 24,499–24,507.

Dieterich, J., V. Cayol, and P. Okubo (2000), The use of earthquake rate changes as a stress meter at Kilauea Volcano, *Nature*, *408*, 457–460.

Dziewonski, A. M., and J. H. Woodhouse (1983), An experiment in systematic study of global seismicity: Centroid-moment tensor solutions for 201 moderate and large earthquakes of 1981, *J. Geophys. Res.*, *88*, 3247–3271.

Dziewonski, A. M., T.-A. Chou, and J. H. Woodhouse (1981), Determination of earthquake source parameters from waveform data for studies of global and regional seismicity, *J. Geophys. Res.*, *86*, 2825–2852.

Dziewonski, A. M., G. Ekström, and M. P. Salganik (1994), Centroid-moment tensor solutions for January–March 1994, *Phys. Earth Planet. Int.*, *86*, 253–261.

Eaton, J. P., and K. J. Murata (1960), How volcanoes grow, *Science*, *132*, 925–938.

Eaton, J. P., D. H. Richter, and H. L. Krivoy (1987), Cycling of magma between the summit reservoir and Kilauea Iki lava lake during the 1959 eruption of Kilauea volcano, *U.S. Geol. Surv. Prof. Pap.*, *1350*, 1307–1335.

Ekström, G. (1989), A very broad band inversion method for the recovery of earthquake source parameters, *Tectonophysics*, *166*, 73–100.

Ekström, G., and M. Nettles (1997), Calibration of the HGLP seismograph network and centroid-moment tensor analysis of significant earthquakes of 1976, *Phys. Earth Planet. Inter.*, *101*, 219–243.

Ekström, G., J. Tromp, and E. W. F. Larson (1997), Measurements and global models of surface wave propagation, *J. Geophys. Res.*, *102*, 8137–8157.

Ekström, G., A. Morelli, E. Boschi, and A. M. Dziewonski (1998), Moment tensor analysis of the central Italy earth-

quake sequence of September–October 1997, *Geophys. Res. Lett.*, *25*, 1971–1974.

Garcia, M., K. H. Rubin, M. D. Norman, J. M. Rhodes, D. W. Graham, D. Muenow, and K. Spencer (1998), Petrology and geochronology of basalt breccia from the 1996 earthquake swarm of Loihi Seamount, Hawaii: Magmatic history of its 1996 eruption, *Bull. Volcanol.*, *59*, 577–592.

Gillard, D., M. Wyss, and J. S. Nakata (1992), A seismotectonic model for western Hawaii based on stress tensor inversion from fault plane solutions, *J. Geophys. Res.*, *97*, 6629–6641.

Gillard, D., A. M. Rubin, and P. Okubo (1996), Highly concentrated seismicity caused by deformation of Kilauea's deep magma system, *Nature*, *384*, 343–346.

Goldstein, P., and B. Chouet (1994), Array measurements and modeling sources of shallow volcanic tremor at Kilauea Volcano, Hawaii, *J. Geophys. Res.*, *99*, 2637–2652.

Got, J.-L., and P. Okubo (2003), New insights into Kilauea's volcano dynamics brought by large-scale relative relocation of microearthquakes, *J. Geophys. Res.*, *108*(B7), 2337, doi:10.1029/2002JB002060.

Got, J.-L., J. Frechet, and F. Klein (1994), Deep fault plane geometry inferred from multiplet relative relocation beneath the south flank of Kilauea, *J. Geophys. Res.*, *99*, 15,375–15,386.

Hartigan, J. A. (1975), *Clustering Algorithms*, 351 pp., John Wiley, Hoboken, N. J.

Hill, D. P., and J. J. Zucca (1987), Geophysical constraints on the structure of Kilauea and Mauna Loa volcanoes and some implications for seismomagmatic processes, in *Volcanism in Hawaii*, edited by R. W. Decker and T. L. Wright, *U.S. Geol. Surv. Prof. Pap.*, *1350*, 903–917.

Jackson, M. D., E. T. Endo, P. T. Delaney, T. Arnadottir, and A. M. Rubin (1992), Ground ruptures of the 1974 and 1983 Kaoiki earthquakes, Mauna Loa volcano, Hawaii, *J. Geophys. Res.*, *97*, 8775–8796.

Jordan, T. H., and K. A. Sverdrup (1981), Teleseismic location techniques and their application to earthquake clusters in the south-central Pacific, *Bull. Seismol. Soc. Am.*, *71*, 1105–1130.

Klein, F. W. (1981), A linear gradient crustal model for south Hawaii, *Bull. Seismol. Soc. Am*, *71*, 1503–1510.

Klein, F. W., and T. L. Wright (2000), Catalog of Hawaiian earthquakes, 1823-1959, *U.S. Geol. Surv. Prof. Pap.*, *1623*, 90 pp.

Klein, F. W., R. Y. Koyanagi, J. Nakata, and W. R. Tanigawa (1987), The seismicity of Kilauea's magma system, in *Volcanism in Hawaii*, edited by R. W. Decker and T. L. Wright, *U.S. Geol. Surv. Prof. Pap.*, *1350*, 1019–1185.

Klein, F. W., A. D. Frankel, C. S. Mueller, R. L. Wesson, and P. G. Okubo (2001), Seismic hazard in Hawaii: High rate of large earthquakes and probabilistic ground-motion maps, *Bull. Seismol. Soc. Am.*, *91*, 479–498.

Koyanagi, R. Y., B. Chouet, and K. Aki (1987), Origin of volcanic tremor in Hawaii, *Volcanism in Hawaii*, edited by R. W. Decker and T. L. Wright, *U.S. Geol. Surv. Prof. Pap.*, *1350*, 1221–1257.

McGovern, P. J., and S. C. Solomon (1993), State of stress, faulting, and eruption characteristics of large volcanoes on Mars, *J. Geophys. Res.*, *98*, 23,553–23,579.

Menke, W. (1999), Using waveform similarity to constrain earthquake locations, *Bull. Seismol. Soc. Am.*, *89*, 1143–1146.

Mooney, W. D., G. Laske, and G. Masters (1998), CRUST-5.1: A global crustal model at 5° × 5°, *J. Geophys. Res.*, *103*, 727–747.

Mori, J., and C. McKee (1987), Outward-dipping ring-fault structure at Rabaul caldera as shown by earthquake locations, *Science*, *235*, 193–197.

Nadeau, R. M., W. Foxall, and T. V. McEvilly (1995), Clustering and periodic recurrence of microearthquakes on the San Andreas fault at Parkfield, California, *Science*, *267*, 503–507.

Nettles, M., and G. Ekström (1998), Faulting mechanism of anomalous earthquakes near Bárdarbunga Volcano, Iceland, *J. Geophys. Res.*, *103*, 17,973–17,983.

Nettles, M., and G. Ekström (2004), Long-period source characteristics of the 1975 Kalapana earthquake, *Bull. Seismol. Soc. Am.*, in press.

Owen, S., P. Segall, J. Freymueller, A. Miklius, R. Denlinger, T. Arnadottir, M. Sako, and R. Bürgmann (1995), Rapid deformation of the south flank of Kilauea volcano, Hawaii, *Science*, *267*, 1328–1332.

Peterson, D. W., and R. B. Moore (1987), Geologic history and evolution of geologic concepts, island of Hawaii, in *Volcanism in Hawaii*, edited by R. W. Decker and T. L. Wright, *U.S. Geol. Surv. Prof. Pap.*, *1350*, 149–189.

Poupinet, G., W. L. Ellsworth, and J. Fréchet (1984), Monitoring velocity variations in the crust using earthquake doublets: an application to the Calaveras fault, California, *J. Geophys. Res.*, *89*, 5719–5731.

Reasenberg, P. A., and D. Oppenheimer (1985), FPFIT, FPPLOT and FPPAGE: Fortran computer programs for calculating and displaying earthquake fault-plane solutions, *U.S. Geol. Surv. Open File Rep.*, *85–739*.

Richards-Dinger, K., and P. Shearer (2000), Earthquake locations in southern California using source-specific station terms, *J. Geophys. Res.*, *105*, 10,939–10,960.

Rubin, A. M., and D. Gillard (1998), Dike-induced earthquakes: Theoretical considerations, *J. Geophys. Res.*, *103*, 10,017–10,030.

Rubin, A. M., D. Gillard, and J.-L. Got (1998), A reinterpretation of seismicity associated with the January 1983 dike intrusion at Kilauea Volcano, Hawaii, *J. Geophys. Res.*, *103*, 10,003–10,015.

Rubin, A. M., D. Gillard, and J.-L. Got (1999), Streaks of microearthquakes along creeping faults, *Nature*, *400*, 635–641.

Ryan, M. P. (1988), The mechanics and three-dimensional internal structure of active magmatic systems: Kilauea volcano, Hawaii, *J. Geophys. Res.*, *93*, 4213–4248.

Scandone, R., and S. D. Malone (1985), Magma supply, magma discharge and readjustment of the feeding system of Mount St. Helens during 1980, *J. Volcanol. Geothem. Res.*, *23*, 239–262.

Shearer, P. (1997), Improving local earthquake locations using the L1 norm and waveform cross-correlation: Application to the Whittier Narrows, California, aftershock sequence, *J. Geophys. Res.*, *102*, 8269–8283.

Shearer, P. M. (1998), Evidence from a cluster of small earthquakes for a fault at 18 km depth beneath Oak Ridge, Southern California, *Bull. Seismol. Soc. Am.*, *88*, 1327–1336.

Shearer, P. M., J. L. Hardebeck, L. Astiz, and K. B. Richards-Dinger (2003), Analysis of similar event clusters in aftershocks of the 1994 Northridge, California, earthquake, *J. Geophys. Res.*, *108*, doi:10.1029/2001JB000685.

Swanson, D. A., W. A. Duffield, and R. S. Fiske (1976), Displacement of the south flank of Kilauea Volcano; the result of forceful intrusion of magma into the rift zones, *U.S. Geol. Surv. Prof. Pap.*, *963*.

Tilling, R., and J. J. Dvorak (1993), Anatomy of a basaltic volcano, *Nature*, *363*, 125–133.

Unger, J. D., and P. L. Ward (1979), A large, deep Hawaiian earthquake: The Honomu, Hawaii event of April 26, 1973, *Bull. Seismol. Soc. Am.*, *69*, 1771–1781.

Waldhauser, F., and W. L. Ellsworth (2000), A double-difference earthquake location algorithm: Method and application to the Northern Hayward Fault, CA, *Bull. Seismol. Soc. Am.*, *90*, 1353–1368.

Wolfe, C. J. (2002), On the mathematics of relocating earthquakes using difference operators, *Bull. Seismol. Soc. Am.*, *92*, 2879–2892.

Wolfe, C. J., P. K. Okubo, and P. M. Shearer (2003), Mantle fault zone beneath Kilauea Volcano, Hawaii, *Science*, *300*, 478–480.

Wyss, M., and R. Y. Koyanagi (1992a), Isoseismal maps, macroseismic epicenters, and estimated magnitudes of historical earthquakes in the Hawaiian Islands, *U.S. Geol. Surv. Bull.*, *2006*, 93 pp.

Wyss, M., and R. Y. Koyanagi (1992b), Seismic gaps in Hawaii, *Bull. Seismol. Soc. Am.*, *82*, 1373–1387.